Geodetic and seismic constraints on some seismogenic zone processes in Costa Rica

Edmundo Norabuena,[1,2] Timothy H. Dixon,[1] Susan Schwartz,[3] Heather DeShon,[3,4] Andrew Newman,[3,5] Marino Protti,[6] Victor Gonzalez,[6] LeRoy Dorman,[7] Ernst R. Flueh,[8] Paul Lundgren,[9] Fred Pollitz,[10] and Dan Sampson[3]

Received 5 December 2003; revised 20 July 2004; accepted 4 August 2004; published 9 November 2004.

[1] New seismic and geodetic data from Costa Rica provide insight into seismogenic zone processes in Central America, where the Cocos and Caribbean plates converge. Seismic data are from combined land and ocean bottom deployments in the Nicoya peninsula in northern Costa Rica and near the Osa peninsula in southern Costa Rica. In Nicoya, inversion of GPS data suggests two locked patches centered at 14 ± 2 and 39 ± 6 km depth. Interplate microseismicity is concentrated in the more freely slipping intermediate zone, suggesting that small interseismic earthquakes may not accurately outline the updip limit of the seismogenic zone, the rupture zone for future large earthquakes, at least over the short (~1 year) observation period. We also estimate northwest motion of a coastal "sliver block" at 8 ± 3 mm/yr, probably related to oblique convergence. In the Osa region to the south, convergence is orthogonal to the trench. Cocos-Caribbean relative motion is partitioned here, with ~8 cm/yr on the Cocos-Panama block boundary (including a component of permanent shortening across the Fila Costeña fold and thrust belt) and ~1 cm/yr on the Panama block–Caribbean boundary. The GPS data suggest that the Cocos plate–Panama block boundary is completely locked from ~10–50 km depth. This large locked zone, as well as associated forearc and back-arc deformation, may be related to subduction of the shallow Cocos Ridge and/or younger lithosphere compared to Nicoya, with consequent higher coupling and compressive stress in the direction of plate convergence. *INDEX TERMS:* 8150 Tectonophysics: Plate boundary—general (3040); 8102 Tectonophysics: Continental contractional orogenic belts; 1208 Geodesy and Gravity: Crustal movements—intraplate (8110); 1243 Geodesy and Gravity: Space geodetic surveys; 7230 Seismology: Seismicity and seismotectonics; *KEYWORDS:* seismogenic zone, Costa Rica, geodetic and seismic

Citation: Norabuena, E., et al. (2004), Geodetic and seismic constraints on some seismogenic zone processes in Costa Rica, *J. Geophys. Res.*, *109*, B11403, doi:10.1029/2003JB002931.

1. Introduction

[2] Subduction zones generate Earth's largest and most destructive earthquakes, and most tsunamis. The earthquakes result from mechanical coupling between underthrusting and overriding plates along the shallow (<50 km depth) portion of a dipping plate interface, accumulation of elastic strain during the interseismic period, and rapid release during an earthquake. Factors affecting coupling and strain accumulation/release are important for understanding seismic and tsunami hazard, the earthquake process, and longer-term geological processes that presumably relate to subduction, such as orogeny, crustal shortening and trench-parallel translation of forearc blocks (terrane migration). Key factors include the efficiency of strain accumulation (locking versus aseismic slip on the plate interface), spatial variations (updip and down-dip limits, along-strike variability) and temporal variation, including changing patterns of strain accumulation during the interseismic part of the earthquake cycle, and rapid seismic versus slow aseismic strain release during and after the coseismic part of the cycle.

[1]Rosenstiel School of Marine and Atmospheric Sciences, University of Miami, Miami, Florida, USA.
[2]Now at Instituto Geofisica del Peru, Lima, Peru.
[3]Earth Sciences Department, University of California, Santa Cruz, California, USA.
[4]Now at Department of Geology and Geophysics, University of Wisconsin-Madison, Madison, Wisconsin, USA.
[5]Now at Los Alamos National Laboratory, Los Alamos, New Mexico, USA.
[6]Observatorio Vulcanológico y Sismológico de Costa Rica, Universidad Nacional, Heredia, Costa Rica.
[7]Scripps Institution of Oceanography, University of California, San Diego, La Jolla, California, USA.
[8]Leibniz Institut fur Meereswissenshaften, Forschungszentrum fur Marine Geowissenschaften (IFM-GEOMAR) and SFB574 Christian-Albrechts Universitat, Kiel, Germany.
[9]Jet Propulsion Laboratory, California Institute of Technology, Pasadena, California, USA.
[10]U.S. Geological Survey, Menlo Park, California, USA.

0148-0227/04/2003JB002931$09.00

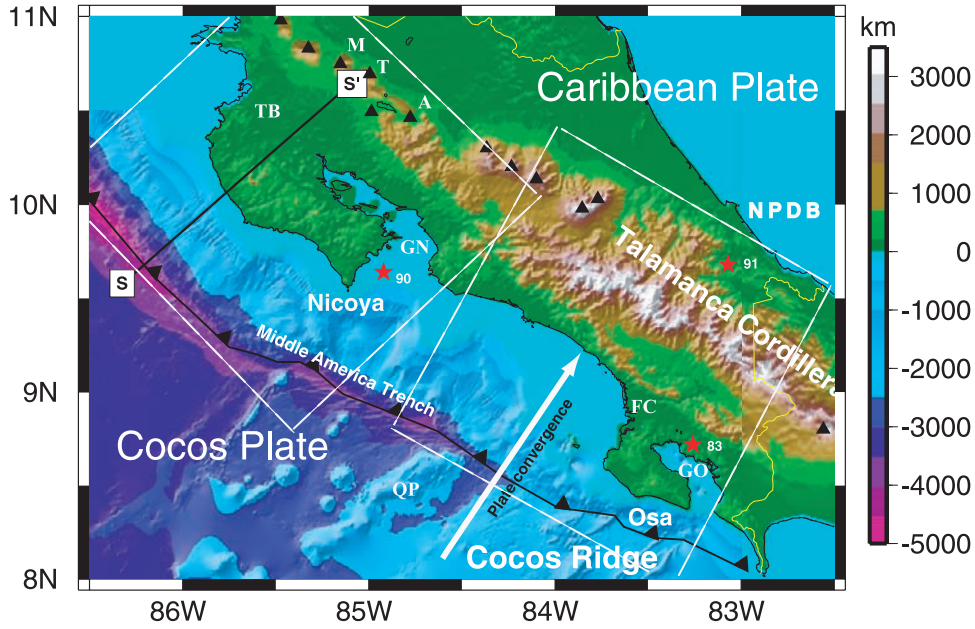

Figure 1. Location map with major physiographic and plate tectonic features of the study area. Arrow shows convergence direction of Cocos plate relative to Caribbean plate. TB is Tempisque Basin, GN is Golfo Nicoya, GO is Golfo Osa, FC is Fila Costeña, QP is Quepos Plateau. NPDB is North Panama Deformed Belt, part of the northern boundary of the Panama block. Volcanoes mentioned in text are Arenal (A), Tenorio (T), and Miravalles (M). Stars mark location of major earthquakes since 1980. Dashed boxes outline areas shown in Figures 3a and 3b. Line S-S′ shows location of seismic line 101 [*Christeson et al.*, 1999; *Sallarès et al.*, 2001] used in Figure 3c.

[3] During the interseismic period, patterns of strain accumulation on the plate interface may be inferred from geodetic data, while the updip and down-dip limits of the seismogenic zone and its overall geometry may be determined from microseismicity. However, interpretations of geodetic data are nonunique, while microseismicity may not adequately delineate the main plate interface and may also exhibit temporal variation, such that short (several years) observation periods yield temporally aliased results. Earthquakes may also be poorly located if local recording stations are limited. Comparison of results from each technique is therefore useful. In this paper we describe results of joint geodetic and seismic observations, part of a large international project we have called the Costa Rica Seismogenic Zone Experiment (CRSEIZE). The observations are designed to elucidate the geometry of the seismogenic zone as well as spatial variations in locking on the plate interface in Costa Rica. Geodetically determined locked and slipping zones on the plate interface are compared with interplate microseismicity (“interseismic earthquakes”) and the aftershock regions of past large earthquakes to better understand the mechanical behavior of the plate interface. We also address possible relations between short-term strain accumulation and longer-term geological processes in the subduction environment. We focus on the Osa and Nicoya peninsulas in southern and northern Costa Rica, respectively, along the Middle America Trench (Figure 1). These peninsulas enable deployment of GPS and seismic equipment close to the trench, immediately above much of the seismogenic zone, a situation that is advantageous for monitoring subduction zone seismicity and strain accumulation. The Costa Rica subduction zone is also a potential target for the Integrated Ocean Drilling Program, to drill into and instrument the seismogenic zone.

2. Tectonic Setting

[4] Figure 1 shows the major tectonic features of the experiment area. The Cocos plate subducts beneath Central America, the leading edge of the Caribbean plate, at rates of 8–9 cm/yr [*DeMets et al.*, 1990, 1994; *Dixon*, 1993; *DeMets*, 2001]. The age of subducted oceanic lithosphere ranges from 15–16 Ma in southern Costa Rica to 22–24 Ma in northern Costa Rica [*Barkhausen et al.*, 2001]. Lithosphere off southern and central Costa Rica was created at the Cocos-Nazca Spreading Center, and has generally rough bathymetry, while lithosphere off northern Costa Rica was created at the East Pacific Rise and is characterized by smooth bathymetry and thicker sediment cover [e.g., *Von Huene et al.*, 1995; *Protti et al.*, 1995b].

[5] Crustal structure and the dip of the shallow portion of the subducted slab in Costa Rica are well characterized based on numerous seismic reflection and refraction studies [e.g., *Ye et al.*, 1996; *Stavenhagen et al.*, 1998; *Christeson et al.*, 1999; *Sallares et al.*, 1999, 2000, 2001]. There are significant geologic contrasts between northern and southern Costa Rica that relate primarily to the dip and age of subducted lithosphere, subduction obliquity, and the presence or absence of anomalous bathymetry on the subducted plate (Figure 2). In southern Costa Rica, subduction is essentially orthogonal to the trench, and the Cocos Ridge,

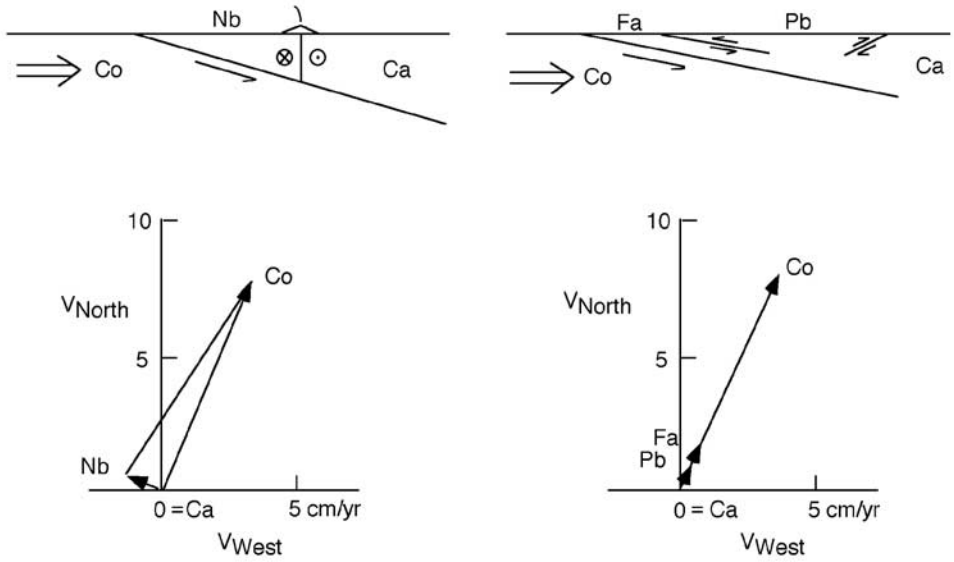

Figure 2. Cartoon comparing block tectonics for northern and southern Costa Rica. (top) Cross sections of plate and block convergence directions. Co is Cocos plate, Ca is Caribbean plate, Nb is Nicoya block, Pb is Panama block, Fa is forearc. (bottom) Representative vector diagrams showing relative plate and block motions in a Caribbean plate reference frame.

an aseismic ridge created at the Galapagos hot spot, subducts beneath the Osa Peninsula. Combined with the young age of subducting lithosphere here, this results in relatively high buoyancy of the subducting slab and a shallow dipping subduction zone. This probably causes or at least influences a number of geologic features, including lack of active arc volcanism, elevation of the Cordillera Talamanca, back-arc shortening along the North Panama deformed belt (NPDB, Figure 1), and development of a separate Panama block. While this block's northern boundary (the NPDB) is well defined, its western boundary in central Costa Rica is poorly defined. In northern Costa Rica, subduction angle is steeper relative to the south and an active volcanic arc is present. All or part of the Nicoya Peninsula may move as a separate block essentially parallel to the trench, associated with a major change in the trend of the Middle America trench and consequent oblique convergence [*Lundgren et al.*, 1999; *McCaffrey*, 2002].

3. Seismic Observations and Results

[6] Given subduction zone geometry, accurate earthquake location may require simultaneous recording of events on land, over the down-dip portion, as well as on the seafloor, near the trench and updip portion. We conducted two seismic campaigns during CRSEIZE, one near the Osa peninsula in southern Costa Rica, and the other on and offshore the Nicoya peninsula in northern Costa Rica (Figure 3). Each campaign included deployment of standard IRIS/PASSCAL three-component broadband as well as short-period seismometers on land, and three-component broadband ocean bottom seismometers (OBS) (improved versions of those described by *Sauter et al.* [1990] and *Jacobson et al.* [1991]) as well as ocean bottom hydrophones (OBH) offshore, with extensive periods of simultaneous observations. Data from two 6-month deployments comprising 23 OBH and 15 short-period land stations each between the Osa and Nicoya peninsulas, operated by SFB 574 of Christian-Albrechts Universitat Kiel and GEOMAR, comprise a total of nearly 10,000 events and are currently being processed. Results and analytical techniques for the U.S. OBS and PASSCAL deployments are given by *Newman et al.* [2002], *DeShon et al.* [2003], and *DeShon* [2004] and summarized here.

[7] The OBS network originally planned for deployment directly offshore the Osa peninsula to coincide with the existing GPS transect (Figure 4) was moved 30 km northwest to take advantage of aftershocks from the 20 August 1999 M_w = 6.9 underthrusting earthquake near Quepos (Figure 3a). Fourteen OBS were deployed by GEOMAR's

Figure 3. Plan view and cross section of seismic stations and earthquake locations for (a) Osa and (b) Nicoya peninsulas. For Osa, star marks location of 20 August 1999 M_w = 6.9 Quepos underthrusting earthquake. For Nicoya, star marks location of 21 July 2000 M_w = 6.4 outer rise earthquake. (c) Vertical cross section of plate boundary beneath Nicoya peninsula along profile S-S′ (Figure 1). Red solid line is based on seismic reflection/refraction study of *Christeson et al.* [1999]; triangles are based on reanalyses by *Sallarès et al.* [2001]; yellow circles are subset of well-located microearthquakes shown in Figure 3b (this study) within ±20 km of the profile, as recorded by ocean floor and land seismic arrays (instruments located between downward pointing blue arrows at 10 km and 145 km; note trench at 20 km); black solid line is plate boundary approximation used for GPS strain modeling; dashed lines denote range of tested models. Plate interface between upward pointing green arrows northeast of trench at 55 km and 80 km (11–18 km depth) is locked by amounts that exceed 50% of plate rate (Figures 13 and 14).

cruise with F/S *Sonne* during leg S0144-1a of the Paganini expedition (San Diego–Punta Caldera) northwest of Osa between 7 and 27 September 1999 [*Bialas et al.*, 1999]). Twelve OBS remained operational during the Osa deployment. The stations were recovered, serviced and redeployed offshore Nicoya by *Sonne* on leg SO144-3b between 3 and 19 December 1999 (Punta Caldera–Balboa). The Nicoya OBS deployment covered a broad area from very nearshore

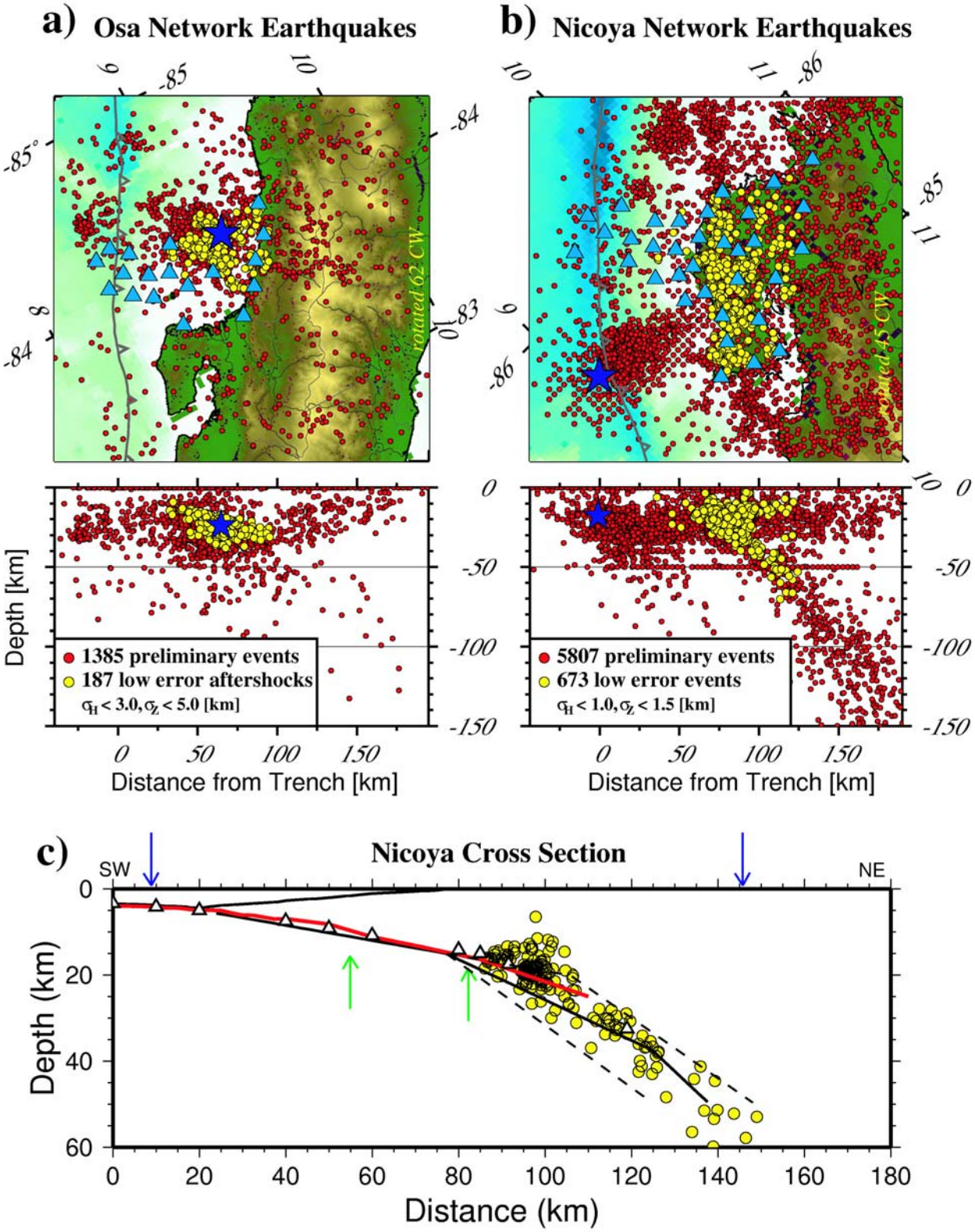

Figure 3

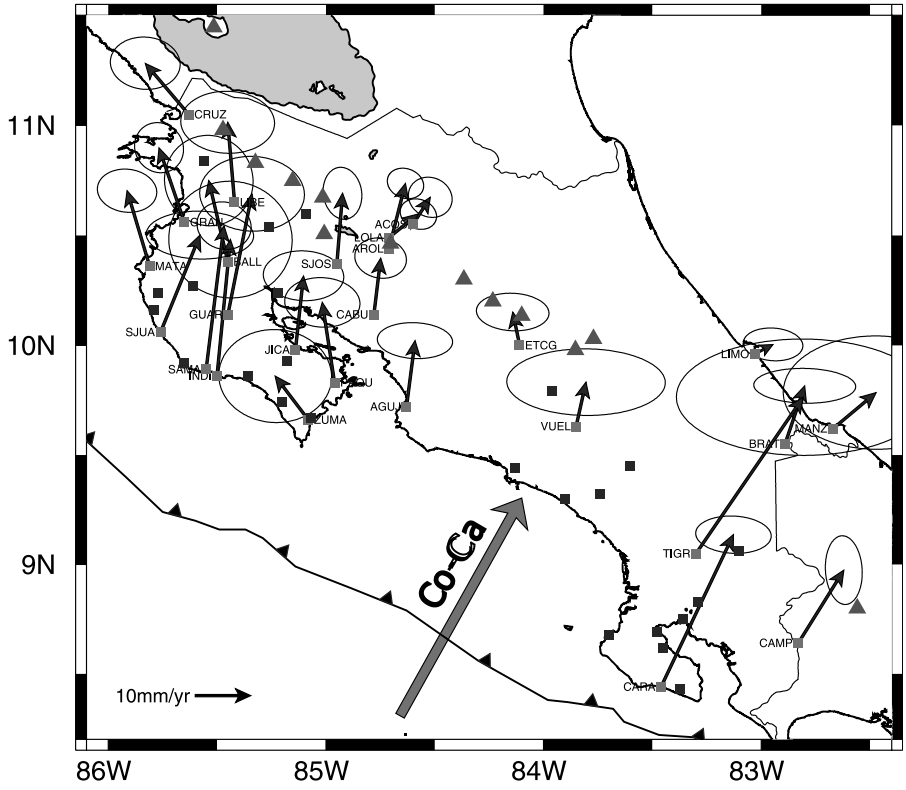

Figure 4. GPS site velocities with respect to the stable Caribbean plate. Sites first occupied in 1994 are gray squares with names, arrows show horizontal component of velocity vectors with 95% confidence ellipses; site first occupied in 2000 (velocities not yet defined) are shown as dark squares. Triangles are active volcanoes. Large arrow (Co-Ca) shows direction of Cocos plate convergence relative to Caribbean plate, with rate at half scale (plate rate here is ~9 cm/yr). In southern Costa Rica, site velocities are parallel to convergence direction; in northern Costa Rica, site velocities are rotated counterclockwise from convergence direction.

to oceanic crust just seaward of the trench. Thirteen OBS remained operational during the Nicoya deployment until recovery by Scripps Institution of Oceanography's R/V *Melville* on cruise NEM004 (Punto Caldera–San Diego) between 12 and 28 June 2000.

[8] During the Osa OBS deployment, six land seismometers (one broadband Streickeisen STS-2 and five short-period three-component instruments) were installed along the Pacific coastline (Figure 3a). All the land stations were operating by 24 September 1999, when most of the OBS were running, and operated through 25 November 1999. The land stations were then redeployed to Nicoya to coincide with the OBS redeployment. During this period, a total of 20 land stations were installed: 10 broadband (5 Streickeisen STS-2, 4 Guralp 3T, 1 Guralp 40T) and 10 short-period instruments. These were distributed throughout the Nicoya peninsula in mid-December 1999 and operated through June 2001 (Figure 3b).

3.1. Osa Seismic Data

[9] The Osa array primarily recorded aftershocks of the 20 August 1999 earthquake, illuminating most of the seismogenic zone northwest of the Osa Peninsula along the northern flank of the subducting Cocos Ridge (Figure 3a). The network recorded more than 1300 regional and local events from mid-September 1999 through early December 1999. *DeShon et al.* [2003] describe processing techniques and details of the seismic deployment and data interpretation. The main results include high-precision absolute and relative relocations of aftershock seismicity that define a 19° dipping plane, interpreted as the Cocos plate–Panama block interface and consistent with wide-angle refraction data for this region [*Stavenhagen et al.*, 1998]. The updip limit of the aftershocks occurs at ~10 km depth below sea level, and the down-dip limit at 30–35 km depth, corresponding to 30–35 km and ~95 km from the trench axis respectively. Aftershocks correlate spatially with the down-dip extension of the Quepos Plateau, a bathymetric high on the incoming Cocos plate (Figure 1), and may reflect the structure of the main shock rupture asperity [*Bilek et al.*, 2003]. Since the geodetic and seismic data for the Osa region are not spatially coincident, the fault plane used for geodetic models cannot be defined solely on the basis of microseismicity, although they provide a useful constraint. Seismic reflection and refraction data exist for the crest of the Cocos Ridge from seaward of the trench to the Osa peninsula coast [*Walther*, 2003], but there are no reflection or refraction seismic data tracing the plate interface beneath the peninsula itself.

3.2. Nicoya Seismic Data

[10] The Nicoya network imaged the Middle America subduction zone offshore northern Costa Rica from seaward of the trench, across the entire Nicoya Peninsula, through to

the Nicoya Gulf (Figures 3b and 3c), recording more than 8000 regional and local earthquakes from December 1999 to June 2001. Experiment details and hypocenter locations obtained with a fixed velocity model are described by *Newman et al.* [2002]. Shallow seismicity beneath the Nicoya Peninsula, both crustal and along the plate interface, represents about 20% of the earthquakes located by *Newman et al.* [2002]. Data analysis originally focused on the 21 July 2000 M_w = 6.4 outer rise earthquake and its aftershocks (Figure 3b). This event was a normal faulting earthquake that ruptured the oceanic crust and possibly into the mantle in the vicinity of the Fisher Seamount Chain [*Schwartz et al.*, 2001]. Pertinent results from this work include observation of deep slab seismicity extending down to 220 km, recorded but not well constrained by the Nicoya network, a large number of well-located interplate and intraplate events shallower than 50 km, and variability in the depth of the shallowest seismogenic zone earthquakes, possibly corresponding to differences in subducted oceanic crust and regional heat flow patterns [*Langseth and Silver*, 1996; *Harris and Wang*, 2002; *Fisher et al.*, 2003; *Walther and Flueh*, 2002].

[11] *DeShon* [2004] relocated earthquakes analyzed to date (almost twice as many events as included in our earlier study [*Newman et al.*, 2002]) using a simultaneous inversion for a minimum one-dimensional *P* and *S* wave velocity model, Nicoya network station corrections, and earthquake locations. The updated Nicoya hypocenters (Figure 3b) are similar to those obtained by *Newman et al.* [2002]. The depths of some of the earthquakes are a few kilometers shallower due to differences in the shallow velocity model used for earthquake location. Figure 3b also shows a subset of well-located events (673 events, RMS < 0.10 s) with a location precision (one standard error) better than 1 km in both horizontal and vertical components.

[12] One important application of our precise earthquake locations is the geometric definition of the plate interface for modeling the geodetic data. Mislocation of this boundary may introduce systematic error in strain accumulation models (a given surface strain signal may reflect partial locking on a shallow interface or full locking on a deeper interface) thus the earthquake data improve the accuracy of the geodetic locking estimates. Figure 3c is a cross section of the Nicoya portion of the plate boundary, showing the model plate interface and supporting data. The shallow (<25 km) plate boundary is clearly identified from seismic reflection and refraction data along profile S-S′ (Figure 1). The locations of well-located events whose hypocenters lie within 20 km of S-S′ are also shown. While there may be slight variations in slab dip along strike beneath Nicoya, a composite surface composed of three planar segments, whose dip increases with depth, fits the reflection/refraction data and the overall seismicity pattern quite well. From the trench axis (~5 km below mean sea level, the datum for all depths reported here) the shallow plane of the model surface closely follows that defined by seismic reflection and refraction, dipping 10° to a depth of 15 km. From 15 to 38 km depth, the intermediate model plane dips at 25°, through a group of hypocenters that delineate a well-defined surface. Beneath 38 km, the dip of the model plane increases to 43°, projecting through the center of a loose cluster of events between 40 and 60 km depth. The spatial distribution of events changes at about 40 km depth: shallower events cluster near the presumed plate interface, while deeper events are more broadly distributed. *Sallarès et al.* [2001] estimate 35–40 km crustal thickness in this region. Hence the transition in seismic behavior may reflect the intersection of the top of the subducting slab with the Moho of the overiding plate [*Ruff and Tichelar*, 1996]. The reduced number of well-located events below ~60 km depth may reflect reduced sensitivity of our array to the deeper plate interface (Figure 3c). We interpret a cluster of shallow (10–15 km) events above the model plane, about 80 km from the trench axis, as upper plate events. We estimate location accuracy (one standard error) of the model plane to be ±2km above 15 km, and ±5 km beneath 15 km. As described below, this uncertainty has a negligible influence on the geodetic model results.

4. Geodetic Observations

[13] *Lundgren et al.* [1999] reported velocities from a geodetic network of 23 GPS sites in Costa Rica, based on campaign observations in 1994, 1996, and (for 12 sites) 1997 (Figure 4). To improve the accuracy of the site velocity estimates, we resurveyed this network in January–February 2000 (3–5 day observations at most sites) using Trimble SSI receivers with Dorn-Margolin antennas and "choke ring backplanes," lengthening the time series by 3–4 years. We also installed and made first epoch position measurements at 20 new sites in Costa Rica (Figure 4). All data from 1994 onward were reanalyzed for this study, using techniques described by *Sella et al.* [2002]. Table 1 lists site locations, velocities for all sites with at least two occupations of a campaign site separated by at least 2 years, or more than 2 years of data for a continuous site, in reference frame ITRF-97 [*Boucher et al.*, 1999], and uncertainties (unless noted, all uncertainties in the text and tables represent one standard error, while velocity error ellipses in figures represent two-dimensional 95% confidence regions). Table 2 lists data quantity and weighted RMS (WRMS) scatter about a best fit line through the daily position estimates, a measure of data quality. Velocity error estimates include the effects of "colored" (time-correlated) noise, following *Mao et al.* [1999] and *Dixon et al.* [2000]. Our vertical velocities are still too imprecise to provide meaningful model constraints (Table 1). Vertical site velocities are listed in Table 1 but not used in subsequent models or discussion.

[14] The WRMS scatter of these data (Table 2) is somewhat higher compared to data acquired by our group in western North America with similar observing times and analytical techniques [e.g., *Dixon et al.*, 2000, 2002]. This may reflect the high and variable wet tropospheric path delay experienced by the microwave GPS signals in the tropical Costa Rica environment (8°–11°N latitude) [*Dixon and Wolf*, 1990], compared to the drier conditions for the cited North American studies (30°–40°N latitude). *Mao et al.* [1999] noted a relation between absolute latitude and noise in GPS velocity estimates, and discussed the possible influence of the tropical troposphere. The larger data set of *Sella et al.* [2002] shows a clear relation between latitude and WRMS scatter, especially for the vertical component. This component is quite sensitive to mismodeling of the

Table 1. GPS Site Velocities Relative to ITRF-97 and Stable Caribbean Plate[a]

				ITRF97[b]			Caribbean[c]	
Station	Latitude, °N	Longitude, °W	Height, m	V_n, mm/yr	V_e, mm/yr	V_v, mm/yr	V_n, mm/yr	V_e, mm/yr
ACOS	10.54	84.60	300	07.5 ± 1.2	17.0 ± 1.5	2.5 ± 3.1	4.9 ± 1.5	3.1 ± 1.6
AGUJ	09.72	84.62	71	14.5 ± 1.0	15.8 ± 2.7	−0.2 ± 2.9	11.9 ± 1.3	1.5 ± 2.8
BALL	10.38	85.44	118	16.9 ± 3.2	10.5 ± 3.2	4.5 ± 6.3	14.6 ± 3.3	−3.5 ± 3.3
CABU	10.13	84.77	499	12.7 ± 1.2	15.3 ± 1.8	−1.6 ± 3.6	10.2 ± 1.5	1.2 ± 1.9
CRUZ	11.05	85.63	267	11.4 ± 1.7	05.8 ± 2.5	−5.1 ± 3.9	9.2 ± 1.9	−7.8 ± 2.6
ETCG	09.99	84.10	1194	08.8 ± 1.1	12.9 ± 2.6	14.7 ± 6.2	6.0 ± 1.4	−1.2 ± 2.7
GRAN	10.56	85.65	122	15.6 ± 1.6	9.3 ± 1.7	0.0 ± 3.1	13.4 ± 1.8	−4.6 ± 1.8
GUAR	10.14	85.44	135	24.0 ± 2.6	18.4 ± 3.8	2.7 ± 4.1	21.8 ± 2.8	4.3 ± 3.9
INDI	09.86	85.50	75	26.8 ± 4.2	16.6 ± 4.5	−10.2 ± 7.1	24.6 ± 4.3	2.4 ± 4.5
JICA	09.97	85.13	61	15.7 ± 1.6	15.6 ± 2.9	−1.1 ± 2.8	13.3 ± 1.8	1.5 ± 3.0
LIBE	10.65	85.42	223	16.7 ± 2.1	12.6 ± 3.4	0.9 ± 6.5	14.4 ± 2.3	−1.2 ± 3.5
MATA	10.35	85.81	78	15.7 ± 1.3	9.9 ± 2.1	0.6 ± 3.3	13.6 ± 1.6	−4.1 ± 2.2
PAQU	09.83	84.95	80	16.9 ± 1.6	12.0 ± 2.7	2.1 ± 4.0	14.4 ± 1.8	−2.2 ± 2.8
SAMA	09.88	85.54	46	28.1 ± 1.5	17.4 ± 1.9	−16.0 ± 4.8	25.9 ± 1.8	3.2 ± 2.0
SJOS	10.36	84.94	1062	15.0 ± 1.6	15.0 ± 1.3	−4.4 ± 4.7	12.7 ± 1.9	1.0 ± 1.4
SJUA	10.06	85.75	44	19.6 ± 1.5	21.2 ± 3.9	−4.7 ± 3.2	17.5 ± 1.8	7.1 ± 3.9
ZUMA	09.65	85.08	214	10.3 ± 3.3	8.3 ± 4.1	−13.1 ± 8.7	7.9 ± 3.4	−6.0 ± 4.1
BRAT	09.55	82.89	60	13.8 ± 1.0	17.9 ± 3.7	−7.8 ± 4.0	10.5 ± 1.3	3.5 ± 3.8
CAMP	08.63	82.83	927	16.5 ± 2.4	23.0 ± 1.2	−1.2 ± 3.9	13.2 ± 2.5	8.2 ± 1.4
CARA	08.44	83.46	18	30.3 ± 1.2	27.4 ± 2.3	4.2 ± 4.1	27.4 ± 1.4	13.0 ± 2.8
LIMO	09.96	83.03	13	5.0 ± 2.1	17.5 ± 3.3	−14.6 ± 6.9	1.7 ± 1.2	3.3 ± 2.2
MANZ	09.61	82.67	185	9.9 ± 4.1	22.1 ± 6.8	−15.1 ± 11.9	6.5 ± 4.2	7.8 ± 6.8
TIGR	09.04	83.29	696	31.3 ± 4.2	33.9 ± 9.3	−10.7 ± 5.7	28.2 ± 4.3	19.3 ± 9.3
VUEL	09.62	83.85	3173	10.9 ± 2.3	16.1 ± 5.8	13.0 ± 5.5	8.0 ± 2.5	1.8 ± 5.8

[a]GPS site velocities are listed alphabetically for northern Costa Rica (ACOS through ZUMA) and southern and central Costa Rica (BRAT to VUEL).
[b]Definition is from *Boucher et al.* [1999].
[c]Definition is based on GPS data of *Sella et al.* [2002].

atmosphere, consistent with the idea that tropical tropospheric effects contribute to higher noise levels of the Costa Rican GPS data. Our model for estimating GPS site velocity uncertainty incorporates these effects to a first approximation, hence geophysical model parameters derived using weighted least squares techniques should not be significantly biased by the higher noise levels.

[15] Table 1 and Figure 4 give horizontal site velocities relative to the Caribbean plate, as defined by *Sella et al.* [2002]. Figure 4 also shows the plate convergence direction, using the Cocos-Caribbean angular velocity vector of *DeMets* [2001] based on geologic data. This model agrees well with the single available measurement of present-day plate motion here (from GPS), 88 mm/yr at an azimuth of N22°E, derived from a baseline that crosses the trench at 8.7°N, between Cocos Island (the only point of land on the Cocos plate) and San Andres Island on the stable interior of the Caribbean plate [*Dixon*, 1993]. Calculated at the same position, the geologic vector is 89 mm/yr at an azimuth of N24°E. While the convergence rate at some other subduction plate boundaries has apparently slowed since Pliocene time [e.g., *Norabuena et al.*, 1999; *Sella et al.*, 2002], the close agreement here between the geodetic measurement averaged over a few years and the corresponding geologic value averaged over several million years suggests remarkably steady convergence, in contrast to the argument of *Murdoch* [2003] that Cocos-Caribbean convergence has recently slowed.

[16] In the Caribbean plate reference frame, site velocities on or near the Caribbean coast that lie on the Panama block can be expected to have residual motion relative to the Caribbean plate, while coastal Caribbean sites to the north, not on the Panama block, should have essentially zero residual motion. Eventually, this velocity differential should allow accurate identification of the northern boundary of the Panama block in central Costa Rica, although the current data set is too sparse. From Figure 4, it is apparent that the velocity field in southern Costa Rica is essentially parallel to plate motion, mainly reflecting elastic strain accumulation on the locked plate interface [e.g., *Savage*, 1983]. In contrast, the velocity field in northern Costa Rica in the vicinity of the Nicoya peninsula displays a counterclock-

Table 2. Data Quantity and Quality

	Time Span,	Number of Data,	WRMS, mm		
Site	years	days	N	E	V
ACOS	6.082	25	4.6	6.9	14.9
AGUJ	6.035	13	8.1	10.0	10.9
BALL	3.203	9	5.9	6.7	13.2
CABU	6.027	14	4.1	7.5	15.3
CRUZ	6.104	14	7.3	10.5	17.2
ETCG	6.254	26	4.6	12.9	33.5
GRAN	6.052	15	6.1	6.8	12.9
GUAR	3.208	10	4.3	8.6	8.3
INDI	2.816	19	8.8	10.1	16.2
JICA	6.049	17	5.3	12.0	11.8
LIBE	3.238	19	4.5	8.2	17.0
MATA	5.997	15	3.9	9.3	13.6
PAQU	6.019	16	5.2	11.7	18.0
SAMA	6.043	15	4.3	8.1	22.3
SJOS	6.038	12	6.2	5.6	20.8
SJUA	6.038	14	4.6	11.1	12.6
ZUMA	1.972	7	3.9	5.5	10.6
BRAT	6.098	11	3.7	14.2	16.5
CAMP	6.084	10	7.7	5.0	15.5
CARA	6.035	11	4.5	9.5	17.2
LIMO	2.035	9	2.7	4.8	8.5
MANZ	2.008	9	4.4	8.6	17.0
TIGR	2.005	7	4.3	11.7	5.7
VUEL	6.027	12	7.9	18.4	24.8

wise rotation of vectors relative to the plate convergence direction, suggesting the influence of one or more additional processes. These processes need to be considered before interpreting the GPS data in terms of strain accumulation on the plate interface.

5. Modeling the Geodetic Data

[17] The surface velocity field measured by GPS represents the integrated effect of a variety of short-term elastic (recoverable) deformation processes and longer-term processes that may permanently deform the upper plate. In order to use the geodetic data to study these processes, we require a model that adequately represents all the significant effects, i.e., those that contribute signal at or above the noise level of the observations, roughly 1–2 mm/yr in horizontal components. This requires some assumptions and simplifications, and consideration of available geologic and seismic constraints. We approximate the complex rheological structure of the region with a simplified rheology, described below, and consider five processes: (1) elastic strain accumulation in the upper plate due to locking on the shallow plate interface, (2) postseismic response to major past earthquakes, (3) trench-parallel motion of a forearc block due to oblique convergence, (4) shortening on out-of-sequence (nonplate boundary) thrust faults and folds in the forearc region, and (5) deformation in the back-arc region.

[18] We assume that processes 1 and 2 result in no long-term deformation of the upper plate. Process 3, while it does involve (or likely involves) elastic deformation, ultimately results in permanent deformation of the upper plate, at rates that may be significant even on geodetic timescales. Similarly, process 4 may involve elastic deformation on out-of-sequence thrust faults, but ultimately results in permanent upper plate shortening. Process 5 may involve both permanent shortening on out-of-sequence thrusts and elastic deformation associated with temporarily locked motion on the Caribbean plate-Panama block boundary, analogous to process 1. For clarity, recall that shortening across a subduction zone as measured by GPS, e.g., between mainland Costa Rica and the center of the Cocos plate [*Dixon*, 1993], represents plate convergence and in that sense is permanent. However, the resultant shortening of the upper plate is mainly elastic, reflecting temporary locking on the main plate boundary thrust that will be released in the next large earthquake. The associated compressive stresses may also drive a small component of permanent deformation (shortening) on nearby out-of-sequence thrusts in the forearc, as evidenced by geologic data, typically a small fraction of the long-term plate convergence rate and often a fraction of the maximum elastic shortening in the upper plate [e.g., *Norabuena et al.*, 1998; *Nicol and Beavan*, 2003]. Similar reasoning applies to motion between the Panama block and the Caribbean plate. In general, separating elastic and permanent shortening may be difficult if the plate boundary and out-of-sequence thrusts are closely spaced, so independent geological information is useful.

[19] We also assume that process interactions can be ignored, i.e., the velocity field reflects the linear superposition of these five processes. Hence their effects can be calculated separately and summed. To further simplify our problem, we split the data set into a southern (Osa) section and a northern (Nicoya) section (there is very little velocity data for central Costa Rica at present). As discussed below, the southern section is affected by processes 1, 2, 4, and 5, while the northern section is affected mainly by processes 1, 2, and 3. Other assumptions and simplifications are described below, as well as a summary of available data constraints.

5.1. Elastic Strain Accumulation From a Locked Plate Boundary

[20] The dominant process affecting the surface velocity field in the region, and the primary focus of this paper, is interseismic strain accumulation associated with a locked plate interface. Over time, earthquakes periodically release accumulated strain, accommodating relative motion between the Cocos and Caribbean plates and the Panama block. The degree of mechanical coupling between the plates (the amount of long-term plate motion or "slip" that is temporarily locked on the plate interface during the interseismic period) affects the rate of strain accumulation. Geodetic studies of subduction zones usually report "locked slip" or "back slip" [*Savage*, 1983] on the plate boundary fault rather than "creep rate," and we follow that convention here; locked slip equal to the full plate or block convergence rate, corrected for shortening on nearby out-of-sequence thrusts, implies a creep rate of zero.

[21] *Lundgren et al.* [1999] presented the first estimates of spatially variable locked slip on the Costa Rica plate interface, and demonstrated significant spatial variation. The improved data set allows us to refine this picture considerably. We assume that strain accumulation can be modeled as a perfectly elastic process, i.e., strain accumulated in the interseismic period is completely released during the subsequent major earthquake, with no permanent deformation of the upper plate. We use the method of *Pollitz et al.* [1998] to investigate the amount of locking and its spatial variation on the seismogenic plate interface, using a constrained inversion of the surface velocity field. Site velocities are inverted to obtain the slip distribution, $s_j(x, y)$ (locked slip), on rectangular fault planes with index j. The slip distribution is parameterized using a set of smooth basis functions (Hermite-Gaussian functions as defined by *Pollitz et al.* [1998]). The maximum likelihood solution is obtained by minimizing a penalty function β:

$$\beta^2 = \chi^2 + \mu\Sigma_j \left|\nabla s_j(x,y)\right|^2,$$

where χ^2 is the data misfit (sum of squared residuals normalized by error squared) and $|\nabla s_j(x, y)|^2$ (smoothness) is a measure of the stability of $s_j(x, y)$, controlled by the damping factor μ.

[22] For Osa, where other relevant data are limited, we approximate the plate interface as a single plane whose long axis is oriented parallel to the mean trench direction, and vary the dip for best fit. For Nicoya, where our new seismic data plus existing reflection/refraction data provide significant constraint, we approximate the plate interface as three adjacent planes, with long axes parallel to the mean trench direction, and dip increasing with depth (Figure 3c). To avoid edge effects, we extend the planes along strike 150 km beyond the study region, defined by data availabil-

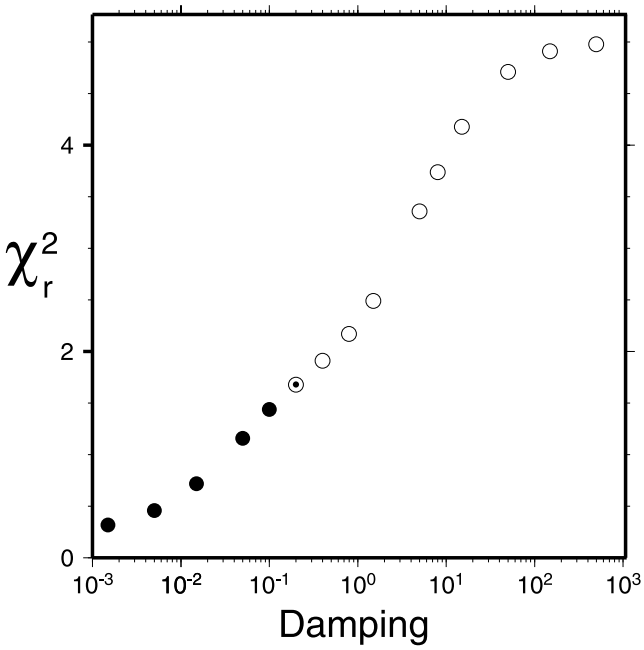

Figure 5. Typical trade-off curve (damping versus misfit, χ^2) for the inversion process. Largest damping value (10^3) gives uniform slip solution. Damping values smaller than 10^{-1} (solid circles) result in low misfit solutions but have negative slip on the fault plane, which may be physically unreasonable. Circled dot represents damping value used for most results in this study.

ity. A given fault plane is parameterized with 120 mutually orthogonal basis functions, so that 120 degrees of freedom per fault plane are available to describe its slip distribution. We impose the constraint that slip at every location on the plane is parallel to the local plate motion; the inversion then gives the amplitude of the slip distribution.

[23] Most models assume a depth extent of the seismogenic plate boundary from 0 to 50 km. To investigate the sensitivity of results to these updip and down-dip boundary conditions, we also tested models with a minimum depth of 15 km, and maximum depths of 42 and 60 km.

[24] Since 120 parameters for a given fault plane greatly exceed the number of data, the inversion is constrained ("damped") to avoid solutions with too many degrees of freedom, and the amount of locked slip on any given patch can vary only slightly from its neighbors (without such constraints, we could obtain essentially perfect fits to the data, but the solutions would not be meaningful). We performed numerical tests to investigate the trade-off between misfit (χ^2) and damping (μ) to find a reasonable value. Figure 5 shows a typical trade-off curve. We did not directly constrain the inversion results to have upper or lower bounds, i.e., the amount of locked slip could exceed the plate rate, or could have negative values. However, since values beyond the plate rate and negative values are physically implausible, we did use these criteria to constrain appropriate damping factors, limiting such extreme values to a small percentage of the overall fault area.

[25] We also performed "checkerboard" tests (Figure 6) to assess the ability of the data to resolve spatial variations in locking for the Nicoya region, where spatial density of GPS sites is relatively high (at present we have much less resolving power for the Osa region due to limited data). First, we assigned contrasting patterns of slip to the fault plane, representing respectively locked and freely slipping patches. Next, we computed the resulting surface displacement at the locations of the GPS sites, and assigned Gaussian noise at the level of 10% of site velocity. We then inverted this synthetic data set using the damping values derived above, solving for slip on the fault plane. Blocks of the size shown in Figure 6 (30 by 40 km) are reasonably well resolved. While there is some "smearing" (the sharp boundary between locked and slipping patches in the synthetic input data is smoothed by the inversion), it is clear that locked patches of the size and location shown can be resolved, and their locations accurately recorded, including offshore patches. Even the updip edge of the synthetic locked patch, 25–35 km offshore, is reasonably well resolved. Before inverting the data to estimate the distribution of locked slip on the plate interface, we first account for other processes affecting the velocity field, as described below.

5.2. Postseismic Motion

[26] Large earthquakes stimulate viscous flow in the lower crust and upper mantle, which in turn affects the surface velocity field via tractions on the upper crust. Postseismic response to smaller events or events far in the past is small and can be ignored. We initially considered the four largest earthquakes in the region in the last 20 years (Table 3) and used the model of *Pollitz* [1997] to estimate corresponding surface displacements during the time frame of GPS observations. Of the four earthquakes considered, only two (1991 Valle de Estrella earthquake in the Osa back-arc region, 1992 Nicaragua earthquake) produced significant displacement at the GPS sites during the observation period for the range of tested rheological models, described below. The calculated postseismic response from these two events is used to "correct" the velocity field prior to estimation of other parameters, as described in the Results section.

[27] While the rheologic structure strongly influences the computed postseismic response, our data are insufficient to invert directly for rheology. Instead, we define a limited number of plausible models based on other information, and use these to compute a series of forward models. Our rheological model consists of three layers in a radially symmetric earth: an elastic upper crust to a depth of 16 km, a Maxwell viscoelastic lower crust to a depth of 30 km, and Maxwell viscoelastic material below, mainly representing the upper mantle (thus we ignore the geometric complexity associated with a dipping subducting plate). *Norabuena* [2004] gives a complete description of the rheological model. *James et al.* [2000] define the average rheology below the crust of the upper plate in the Cascadia subduction zone (i.e., a region that includes the mantle wedge as well as the crust and upper mantle of the subducted plate), using Holocene relative sea level data describing the regional history of postglacial rebound. They infer a mean viscosity of 10^{19} Pa s, considerably smaller than upper mantle values for the interior of North America based on glacial isostatic adjustment (10^{20}–10^{21} Pa s [e.g.,

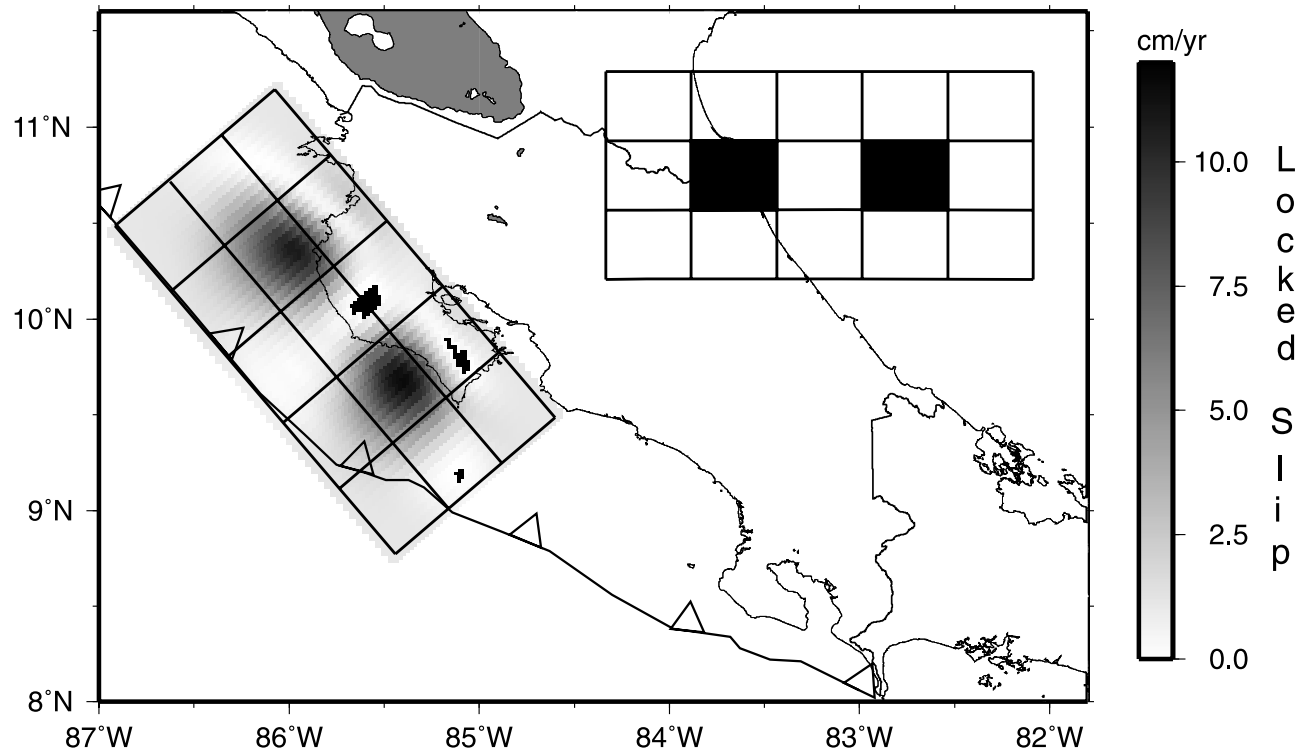

Figure 6. "Checkerboard" test for resolution of slip patches located offshore on main subduction thrust fault in the Nicoya area. Input slip distribution (displaced to upper right for clarity) consists of two locked patches, with 10 cm/yr of locked slip, surrounded by freely slipping zones. Output of inversion is shown in proper geographic position. Three small irregular black patches in output represent regions where inferred slip is negative.

Peltier, 1998]). This may reflect the addition of water to the upper mantle wedge during subduction [e.g., *Peacock*, 1993], which significantly weakens olivine rheology [*Kohlstedt et al.*, 1995; *Hirth and Kohlstedt*, 1996] and/or a weak subducted plate. We tested values of lower crust and upper mantle viscosity of 10^{18}, 10^{19}, and 10^{20} Pa s, for a total of 9 rheological models (3 lower crustal values $\times$ 3 upper mantle values).

5.3. Trench-Parallel Motion of a Forearc "Sliver" Block

[28] Many subduction zones experience oblique convergence, where the plate convergence direction differs from trench-normal direction. Trench-parallel motion of forearc crustal blocks in response to the resulting shear stress is an important aspect of crustal deformation [*Fitch*, 1972; *Jarrard*, 1986], results in permanent deformation of the upper plate, and may be an important mechanism for generation of "exotic terranes" in the outboard parts of continents [*Beck*, 1991; *Beck et al.*, 1994].

[29] Parts of Central America experience northwest translation of coastal regions due to oblique convergence [*DeMets*, 2001; *McCaffrey*, 2002]. Motion of these blocks, located between the trench and the volcanic arc, is likely to be significant in areas of rapid subduction and high obliquity, especially where young lithosphere is subducted and mechanical coupling between subducting and overriding plates is likely to be high [*Beck*, 1991; *McCaffrey*, 1992]. In Central America, obliquity varies due primarily to changes in the trend of the trench. Using new compilations

Table 3. Large Earthquakes Since 1980 in Costa Rica and Nicaragua[a]

Date	Latitude, °N	Longitude, °W	Depth, km	M_w	Strike	Dip	Rake	M_0, N m	Location
3 April 1983[b]	8.72	83.26	26	7.4	310	25	110	1.8×10^{20}	Costa Rica (Osa)
25 March 1990[c]	9.64	84.92	20	7.3	303	11	104	1.1×10^{20}	Costa Rica (Nicoya)
22 April 1991[d]	10.10	82.77	15	7.7	103	25	58	3.3×10^{20}	Costa Rica (Limon)
2 Sept. 1992[e]	11.76	87.41	10	7.6	303	12	91	3.3×10^{20}	Nicaragua

[a]Seismic moment (M_0), moment magnitude (M_w), and other source parameters from Harvard CMT catalog. Strike and dip in degrees, strike measured clockwise from north; rake (degrees) defined such that 90° represents pure reverse slip.
[b]Geographical coordinates and depth from *Adamek et al.* [1987].
[c]Geographical coordinates and depth from *Protti et al.* [1995a].
[d]Geographical coordinates and depth from *Protti et al.* [1994].
[e]Geographical coordinates and depth from USGS NEIC.

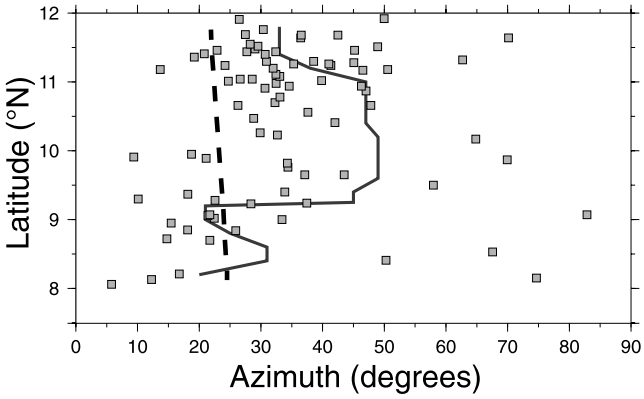

Figure 7. Azimuths of earthquake slip vectors (degrees from north) for plate boundary events for Costa Rica and southern Nicaragua (solid squares) from the Harvard CMT catalog, compared to the azimuth of plate convergence (dashed line from *DeMets* [2001]) and the trench-normal (solid line). South of about 9°N, the trench-normal and the convergence directions coincide (convergence orthogonal to the trench). Between 9°N and 11°N, plate convergence is about 25° oblique, and many earthquake slip vectors are intermediate between the convergence direction and the trench-normal direction.

of bathymetric data [*Ranero and von Huene*, 2000] and the plate motion model of *DeMets* [2001], we computed subduction obliquity for the Middle America Trench offshore Costa Rica (Figure 7). Obliquity varies from essentially zero (orthogonal subduction) in southern and central Costa Rica to about 20° in the northern and central Nicoya peninsula. Although slip vector azimuths of plate boundary earthquakes in Costa Rica appear to be rotated clockwise from the plate convergence direction in the Nicoya region (latitude range ~9–10.5°N), consistent with northwest block motion, there is considerable data scatter (Figure 7) and a precise estimate of Nicoya block translation rate from these data alone is not possible. In part, this reflects limitations in the azimuthal distribution of the global seismic network at the time these earthquakes occurred.

[30] GPS vectors in the Nicoya region exhibit significant counterclockwise rotation relative to the plate convergence direction and relative to observed directions in the Osa region, consistent with northwest translation of a sliver block in the former, and no such motion in the latter. We first compute synthetic velocity fields for various postseismic response models (section 5.2), compute synthetic velocity fields for various models of sliver transport (0–16 mm/yr of northwest translation, assuming a simple elastic half-space model and a single hypothetical strike-slip fault through the volcanic arc that accommodates block motion, locked to a depth of 10 km), correct the observed velocity field for both model processes to derive a residual field that mainly reflects elastic strain accumulation on the plate boundary, and invert this residual field as described in section 5.1. The process is repeated for all possible model combinations, defining a series of satisfactory (low-misfit) models. The models are nonunique because various combinations of parameters may yield similar low-misfit models that are statistically indistinguishable. We can nevertheless define an acceptable range of models, estimating block translation rate and its uncertainty.

5.4. Forearc Shortening

[31] In southern Costa Rica, long-term shortening is accommodated within the Fila Costeña on the Pacific coast. *Fisher et al.* [2004] document a minimum of 3.5–8.7 mm/yr average shortening in the last 2–5 Myr across this fold and thrust belt. In the discussion below, we assume a value of 1 cm/yr. Only the southern part of the GPS data set is affected by this process; similar forearc belts have not been identified north of about 10°N.

5.5. Back-Arc Deformation

[32] In southern Costa Rica, elastic and permanent deformation (shortening) also occur in the back-arc region, on and near the North Panama deformed belt, a fold and thrust belt marking the boundary between the Caribbean plate and the Panama block [*Case and Holcomb*, 1980; *Adamek et al.*, 1987; *Vergara-Munoz*, 1988; *Silver et al.*, 1990, 1995] (Figures 1 and 2). The 1991 M_w = 7.6 Valle de Estrella earthquake was a thrust fault earthquake on a southwest dipping fault defining the northeast corner of the belt, indicating that this boundary is active [*Plafker and Ward*, 1992; *Goes et al.*, 1993; *Lundgren et al.*, 1993; *Protti and Schwartz*, 1994]. Determining the long-term angular velocity of a separate Panama block relative to the Caribbean and Cocos plates is difficult with the current sparse data set.

6. Results of Geodetic Models

6.1. Osa Peninsula

[33] The major processes affecting GPS velocities in southern Costa Rica are (1) elastic strain accumulation on the locked plate interface, (2) postseismic response to the 1991 Valle de Estrella M_w = 7.7 earthquake, (3) permanent shortening in the forearc, and (4) elastic and permanent deformation in the back arc. We first correct the velocity field for the postseismic response 2, then solve for plate boundary and back-arc deformation (1 and 4) by estimating the amount of locked slip on two thrust faults with opposing dips (Figure 2) in a simultaneous inversion. We then consider the effects of forearc shortening (3) on the interpretation of results. GPS data in the Osa region are too sparse to reliably resolve spatially variable slip on the plate boundary. For consistency with the Nicoya results, we show a solution with similar damping (Figure 8), but only the mean locked slip (Table 4) is well constrained.

[34] For the 1991 earthquake we used the source model of *Plafker and Ward* [1992] to predict postseismic motions, and subtracted them from our observations. The geometry of the Panama block–Caribbean plate boundary was based on the work of *Protti and Schwartz* [1994] and *Schwartz* [1995], oriented with its long axis perpendicular to plate motion and dipping 20° southwest. The model plane has a sharp northwest boundary as indicated in Figure 8, but in fact, this boundary is not well defined. To avoid edge effects, the plane extends 150 km southeast of the study area at constant strike and dip. This agrees only approximately with geological studies, but our results are not sensitive to this aspect of the model

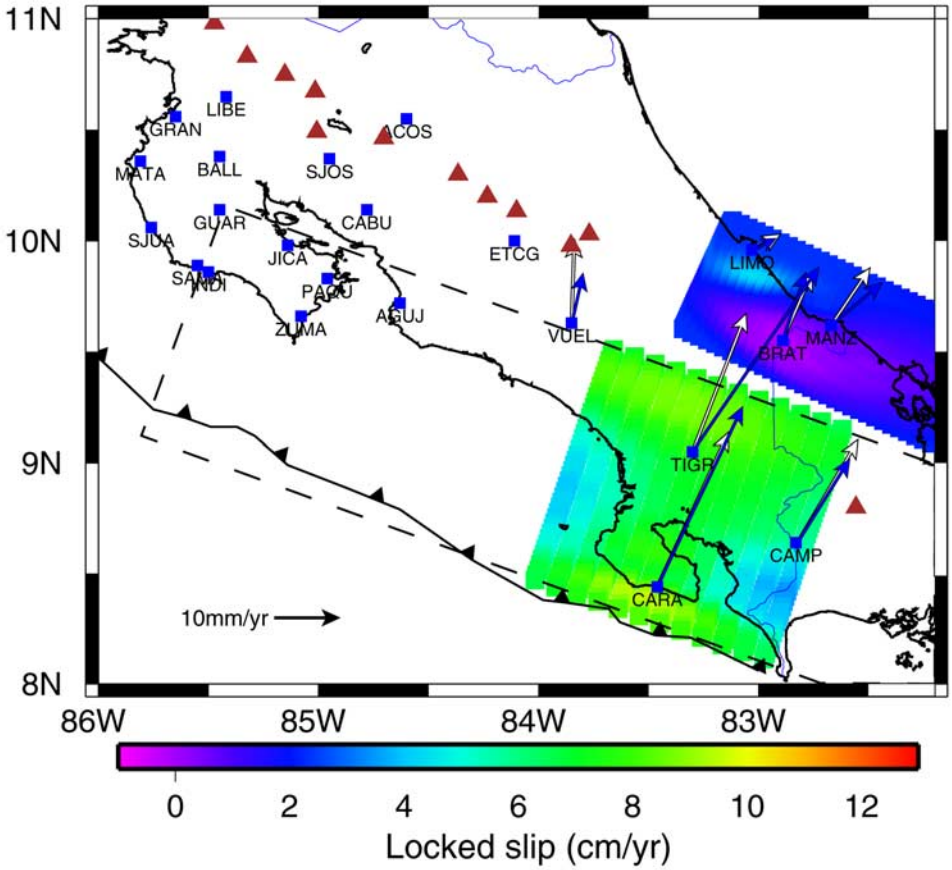

Figure 8. Best fit model for locked slip in the Osa region. Red triangles are active volcanoes. Model fault planes (dashed lines) are colored in region where data density is sufficient to provide some constraint (resolution decreases with distance from GPS site). Main plate boundary model plane (larger rectangle) extends northwest and southeast of data availability to avoid edge effects; back-arc plane extends only to southeast. Observed and calculated GPS site velocities are blue and white. Patch of high locked slip near Pacific coast may be an artifact related to anomalously high velocity at site CARA.

since we have no data there. Site LIMO (Limon) is near the northwest boundary of the block [*Marshall et al.*, 2000] and hence may be sensitive to edge effects. The main plate boundary is treated as a single plane, with dip varied for best fit. We used 19° for the results presented here, but dips between 12° and 22° fit the data acceptably well.

[35] Overall plate convergence here (Cocos-Caribbean relative motion) can be considered partitioned between the Cocos plate–Panama block and Panama block–Caribbean plate boundaries. The inversion results suggest that the Cocos-Panama boundary is accumulating ~8 cm/yr of locked slip, while the Panama-Caribbean boundary is accumulating ~1 cm/yr of locked slip (Figure 8 and Table 4). The sum of these gives the total (Cocos-Caribbean) convergence, ~9 cm/yr. A patch of anomalous slip near site LIMO may reflect edge effects associated with the

Table 4. Comparison of Geodetic and Geologic Characteristics of Osa and Nicoya

	Nicoya	Osa
Maximum locked slip on plate boundary,[a] cm/yr	5.6	8
Mean locked slip,[a,b] cm/yr	3.1	7
Forearc shortening	no	yes
Back-arc deformation	no	yes
Mean locked slip on plate boundary divided by plate rate,[a,b] %	36 ± 3	78 ± 10
High topography	no	yes
Trench parallel block motion	yes	no
Active volcanism	yes	no
Age of subducting seafloor, Ma	22–24	15–16
Bathymetry of subducted seafloor	normal	shallow (Cocos Ridge)

[a]For Osa, Cocos plate–Panama block motion, assuming 1 cm/yr of permanent shortening across the Fila Costeña.
[b]Calculated for depth range 10–50 km.

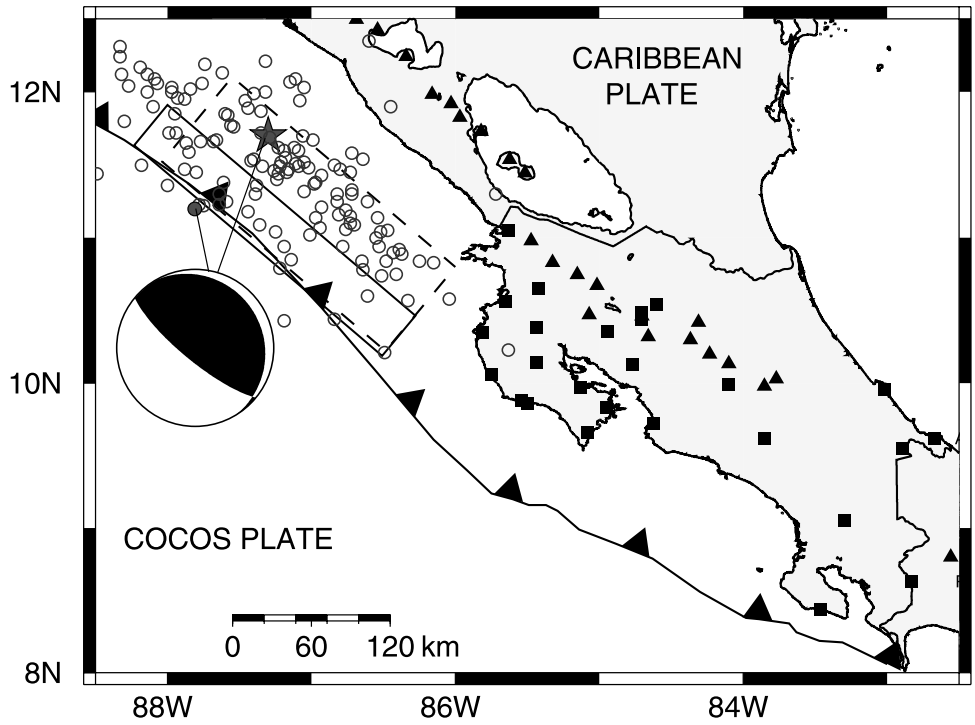

Figure 9. GPS site distribution in Costa Rica compared to rupture area of the 1992 Nicaragua tsunami earthquake. Star is earthquake epicenter (location of initial rupture) from NEIC, estimated from first motion data, and corresponding focal mechanism. Solid circle is from Harvard CMT catalog and represents location of maximum energy release. Difference between these locations is consistent with slow updip rupture and tsunami generation. Open circles are aftershocks from first 30 days (NEIC). Dashed rectangle is our estimate of rupture plane based on these aftershocks. Solid rectangle is rupture plane based on tsunami model [*Satake*, 1994]. GPS sites in northern Costa Rica (squares) are near the southern part of both rupture models.

Panama block boundary. A small patch of high locked slip on the Pacific coast (exceeding the plate rate) is probably an artifact of our limited data. The estimates of locked slip on the plate or block boundaries in the Osa region are based on a sparse data set that is essentially a transect. Hence the estimates have little validity northwest or southeast of the transect, beyond about 20–30 km on either side of the transect line.

[36] The inversion results represent elastic deformation on the main plate or block boundary as well as permanent shortening on nearby structures. For the main plate boundary, we can estimate the magnitude of this effect using available geologic data. Assuming 1 cm/yr of permanent shortening across the Fila Costeña [*Fisher et al.*, 2004] implies 7 cm/yr of elastic locked slip on the main Cocos-Panama boundary, to be released in a future earthquake. Analogous information is not available for the back-arc region. Additional observations at all available sites (Figure 4), explicit inclusion of Fila Costeña structures in the models, and a refined boundary for the Panama block, are needed to improve these results.

6.2. Nicoya Peninsula

[37] The major processes affecting the surface velocity field in northern Costa Rica are (1) elastic strain accumulation on the locked plate interface, (2) trench-parallel motion of the forearc block due to oblique convergence, and (3) postseismic response to the 1992 Nicaragua tsunami earthquake. We first correct the velocity field for the postseismic response, then estimate motion of the forearc block and patterns of locked slip on the plate interface. Since geodetic data density is much higher compared to Osa (Figure 4), the spatial distribution of locking on the plate interface beneath Nicoya is well resolved.

[38] The 1992 Nicaragua earthquake had a very slow rupture, around 100 s, and caused a tsunami much greater than expected for its surface wave magnitude (M_s = 7.2) [*Ide et al.*, 1993]. Using *Kanamori*'s [1972] terminology, this event may be described as a tsunami earthquake [*Kanamori and Kikuchi*, 1993; *Kikuchi and Kanamori*, 1995]. There are significant differences in published estimates of rupture area for this event, which may reflect the slow rupture and corresponding differences in energy release in different frequency bands. *Satake* [1994, 1995] used tide gauge data and tsunami run-up heights to invert for fault rupture, determining a relatively narrow band of coseismic slip starting at the trench, extending 250 km parallel to the trench and 40 km down-dip. Aftershocks define a considerably larger rupture area, extending down-dip to much greater depth. This suggests that afterslip extended the total rupture area to deeper depths. Figure 9 shows the fault plane inferred from tsunami studies [*Satake*, 1994] (hereinafter termed the tsunami model), all aftershocks up to 30 days after the event, and our approximation of the larger fault area as a rectangular plane based on these aftershocks, hereafter termed the aftershock model, similar to the plane defined by *Ihmlé*

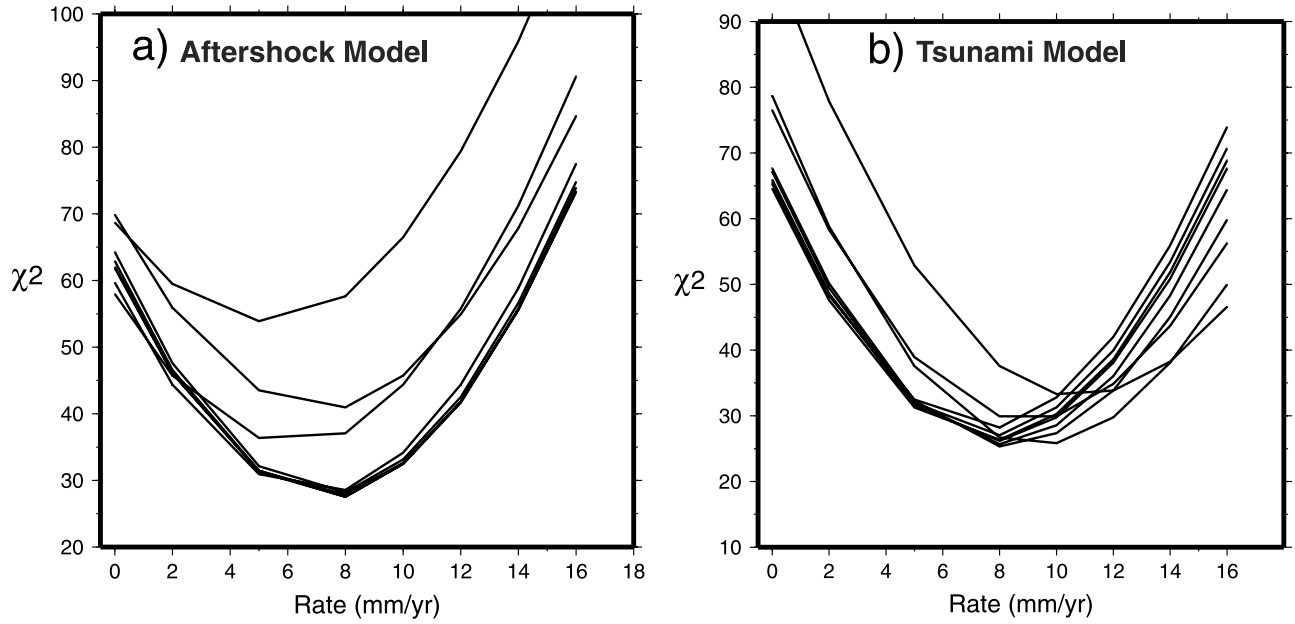

Figure 10. Misfit (χ^2) versus trench-parallel translation rate for the Nicoya block, for 10 low misfit models of postseismic response from the 1992 Nicaragua tsunami earthquake (see Figure 9). (a) Fault plane defined by aftershocks. Best fit model has viscosity of 10^{19} Pa s (lower crust) and 10^{20} Pa s (upper mantle), fault slip 3–5 m; models with upper mantle viscosity of 10^{19} Pa s fit the data nearly as well. (b) Fault plane defined by tsunami model. Best fit model has viscosities of 10^{18} Pa s (lower crust) and 10^{20} Pa s (upper mantle) and fault slip of 3 m; models with lower crust and upper mantle viscosities of 10^{18} and 10^{19} Pa s, respectively, and fault slip of 1m fit the data nearly as well. There is a well-defined minimum at 8 mm/yr regardless of earthquake or rheological model. Uncertainty can be estimated by arbitrarily taking χ^2 value 10% larger than the minimum χ^2, giving ±3 mm/yr.

[1996] based on 90 days of aftershocks. Both the tsunami and aftershock model fault planes are used to generate a series of postseismic response models.

[39] The computed postseismic response is proportional to seismic moment, and hence is sensitive to fault slip for a given fault area. Estimates of the mean slip for the 1992 Nicaragua event vary by nearly an order of magnitude (e.g., 0.38 m [*Imamura et al.*, 1993] and 3.0 m [*Satake*, 1994] reflecting the uncertainty of the fault area and the slow rupture characteristics of this event (estimates of seismic moment vary less). The higher dislocation values are based on tsunami models. The postseismic response is sensitive to the total slip, including afterslip that may have accumulated in the weeks and months following the main shock, which is not reflected in either the seismic or tsunami models. We tested models with 1.0, 3.0, and 5.0 m of slip and thus considered a total of 54 postseismic response models for the 1992 event (9 rheological models × 2 fault planes × 3 mean slip values). For all tested models, the computed postseismic response to the 1992 earthquake at the GPS sites in the middle of the observation epoch (1997) was typically less than 2 mm/yr, although the spatial patterns of deformation varied considerably.

[40] Figure 10 plots the chi-square misfit for the ten lowest misfit models for both the aftershock and tsunami models as a function of northwest block translation rate, showing a well-defined minimum at 8 ± 3 mm/yr. Figure 11 shows the inferred slip distribution on the Nicoya portion of the plate boundary fault for the best fitting (minimum chi-square) solution, and the corresponding observed and calculated velocity vector (the model velocity includes the effects of 8 mm/yr of northwest block motion and postseismic response, as described above). The slip distribution shows two patches of locked slip, with the maximum (~6 cm/yr) centered at 14 ± 2 km depth, and a lower one (~3 cm/yr) at 39 ± 6 km depth, separated by a region of lower locking (~2–3 cm/yr from 22 to 30 km depth) centered at 24 km depth. Locking shallower than 5–10 km may also occur [cf. *Wang and Dixon*, 2004] but would be difficult to detect with the current data. On the basis of the checkerboard resolution test, the locked patches could either represent the gradational distribution illustrated, or perhaps two smaller, fully locked patches separated by a freely slipping region. This is better illustrated in Figure 12, where we adjust the size and position of two small, fully locked input patches in a checkerboard test to yield an output that roughly matches results of the data inversion. Thus the current data cannot distinguish between gradational variations in locked slip and a more abrupt pattern of locked and freely slipping zones.

[41] The occurrence of two patches of locked slip near the updip and down-dip limits of the seismogenic zone is present in all of the low-misfit models for Nicoya. We tested the robustness of this result in several ways. In terms of sensitivity to postseismic models, Figure 13 plots the amount of locked slip on the seismogenic zone as a function of depth, for the 10 lowest misfit models, for both the aftershock and tsunami models of the 1992 earthquake fault plane. Also shown is a reference line showing 50% of the plate convergence rate (4.3 cm/yr at this location). Locked

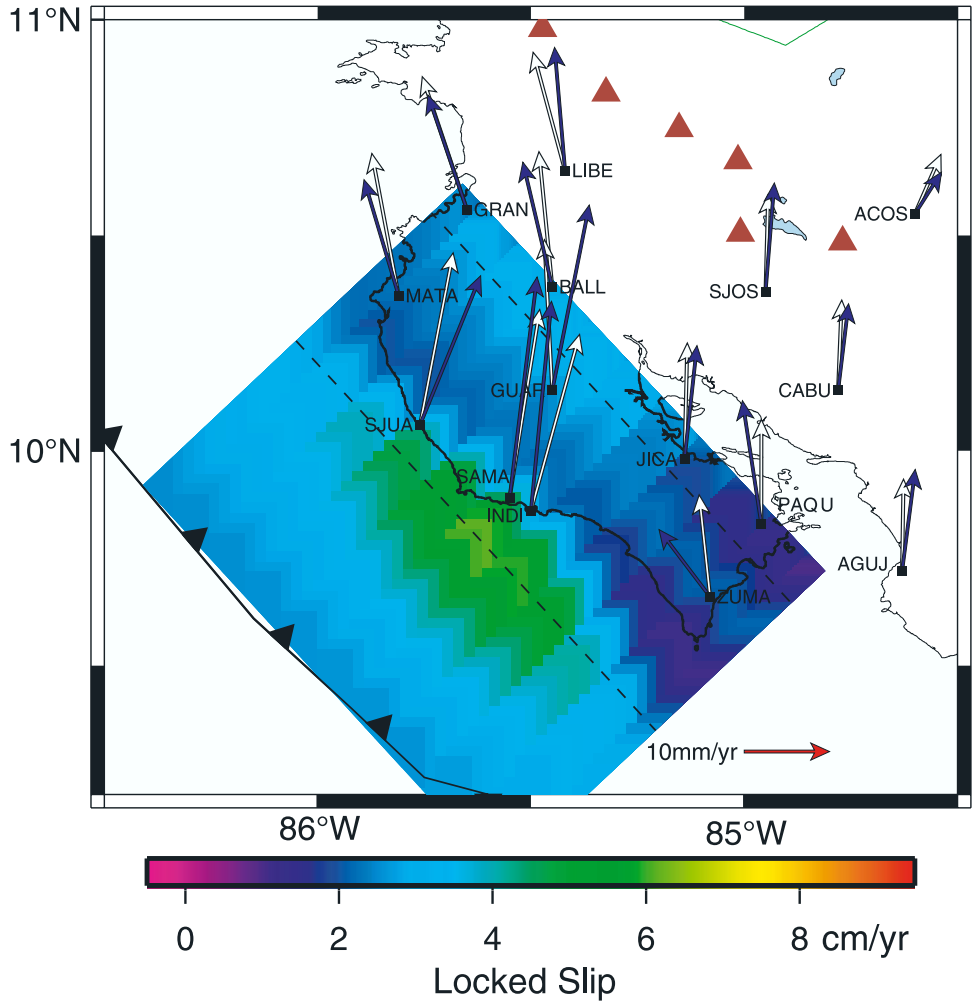

Figure 11. Best fit model for locked slip on plate interface, Nicoya region. Observed and calculated GPS site velocities are blue and white, and red triangles are active volcanoes. Light dashed lines parallel to trench show boundaries of three adjacent subplanes in model plate interface, with increasing dip to northeast (Figure 3c). Model plane is colored where data density provides some resolution for locking estimate (resolution decreases with distance from GPS sites) but extends northwest and southeast to avoid edge effects. Note elliptical locked patch (maximum of 5.6 cm/yr of locked slip) just offshore, elongated parallel to the trench, and a second patch near the down-dip limit (maximum of 3.5 cm/yr).

slip exceeding 50% of the plate rate occurs only in a narrow depth range on the plate interface, ~11–18 km. All of the geodetic model results have locked slip that peaks at about 14 km depth, although the maximum amount of locked slip varies slightly with the various models, between ~5 and 7 cm/yr.

[42] We tested the sensitivity of the locking pattern to possibly erroneous data at individual sites by successively eliminating a data point and reinverting the edited data set (Figure 14). In all cases the overall pattern of two highly locked patches is retained, although the maximum and minimum amplitudes vary slightly. The largest variation is observed when site ZUMA is removed, but even here the key results noted above persist.

[43] The three dimensional location of the model plate interface may also influence the estimated locking pattern. We tested the sensitivity of results to systematic errors in the location of this interface in several ways. First, we defined two other model plate interfaces, along the upper and lower surface of interplate microseismicity in the depth range 15–50 km, i.e., above and below what we believe to be the optimum interface (Figure 3c). In both cases the shallow locked patch remains, at about the same distance from the trench. We also ran a test where the uppermost fault plane was eliminated, forcing all the locked slip to be distributed on the two deeper planes. Data misfit increased significantly, regardless of rheological model, but the peak in locked slip for the shallow locked patch remained shallow, at the top of the remaining two planes. A test of the sensitivity of the deeper locked patch to the down-dip extent of the model interface suggests that results do have some sensitivity to this parameter. For example, extending the model plane from 50 km to 60 km depth reduces the peak magnitude of locked slip from 3.5 to 2.7 cm/yr, although the general location of the deeper locked patch is not affected (Figure 15). For all tested models, the down-dip limit of

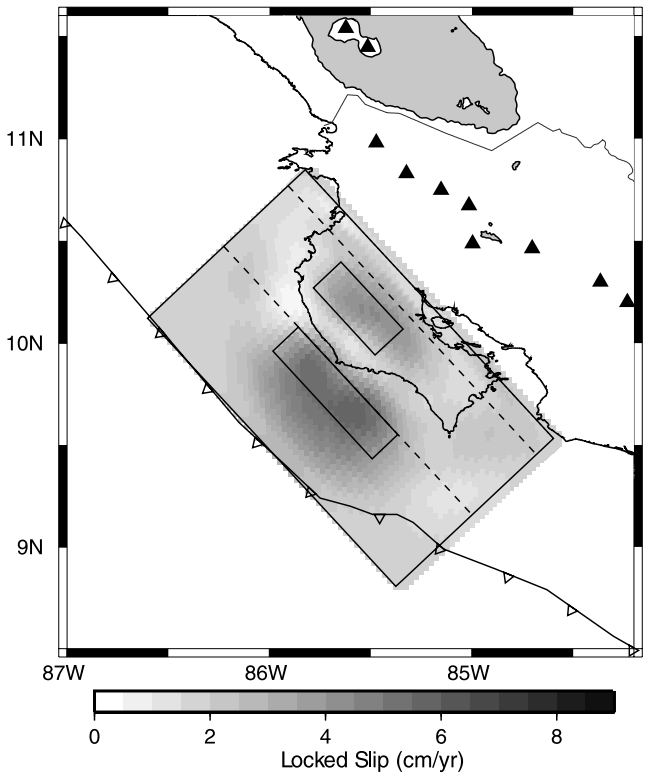

Figure 12. Checkerboard test to yield output similar to data inversion results. Rectangles outline areas of locked slip on plate boundary used as input to inversion (top rectangle 20 by 80 km, 9 cm/yr of locked slip; bottom rectangle 50 by 23 km, 4.5 cm/yr of locked slip); shading indicates output for comparison to Figure 11.

locking (i.e., locked slip less than about 2 cm/yr) approximately coincides with the down-dip rupture limit of past earthquakes (Figure 16).

[44] In summary, the overall pattern of shallow locked slip is a robust result and is not sensitive to model details. The magnitude and extent of the deeper locked patch exhibit some sensitivity to the assumed down-dip extent of locking, but coincides with the rupture limit of past large earthquakes, suggesting that it is a real feature.

7. Discussion

7.1. Updip and Down-Dip Limits of the Seismogenic Zone

[45] The updip limit of the seismogenic zone is often defined on the basis of interseismic microearthquakes [e.g., *Newman et al.*, 2002; *Obana et al.*, 2003] and compared to other geophysical quantities, e.g., thermal state, and laboratory data on the stability of different minerals as a function of pressure and temperature, in order to elucidate seismogenic processes [*Hyndman et al.*, 1995; *Hyndman and Wang*, 1995]. One of the motivations of our study was to compare the updip and down-dip limits of the seismogenic zone as defined from interseismic microearthquakes and geodesy. In the Nicoya region both data sets are large enough to make the comparison meaningful. Figures 16 and 17 suggest that the microseismic and geodetic definitions of the updip limit here do not agree, at least for the time span sampled by our data. The geodetic data show an increase in locked slip beginning about 25 km inland from the trench (~8 km depth), and a clear peak in locked slip 50 km from the trench (14 km depth), in approximate agreement with the updip rupture limit of past large earthquakes, but considerably updip from the beginning of microseismicity, 65 km from the trench (~16 km depth). The distinctive patterns of locking and

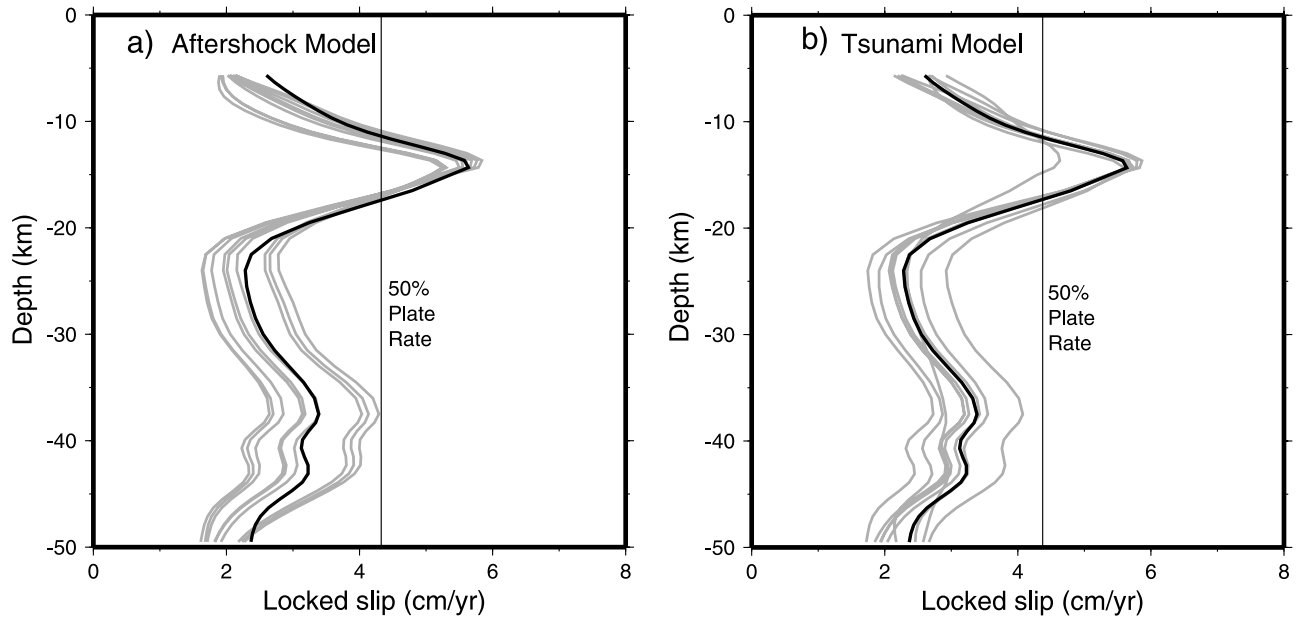

Figure 13. Ten lowest misfit model for locked slip on the plate boundary versus depth, Nicoya peninsula, for (a) aftershock and (b) tsunami models of postseismic response from the 1992 Nicaragua tsunami earthquake (Figure 9). Heavy line indicates best fit model.

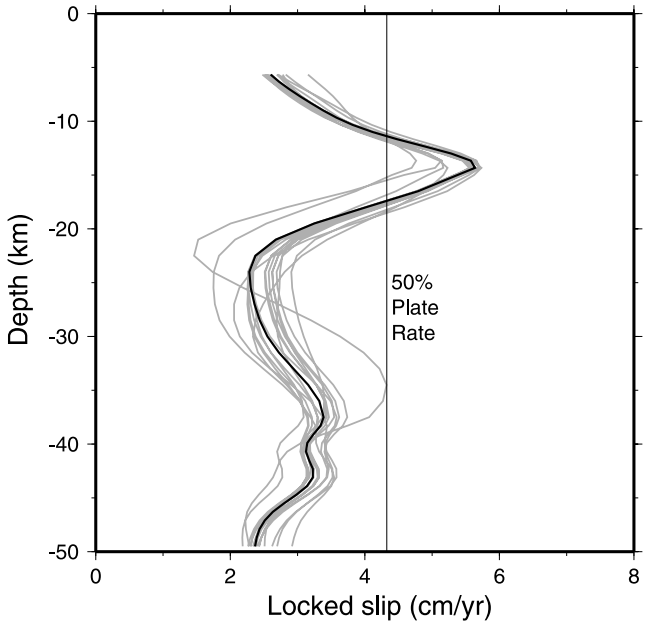

Figure 14. Similar to Figure 13, showing sensitivity of inversion to data at individual GPS sites. Best fit postseismic model and block translation rate are assumed. Successive data points in the Nicoya region are eliminated, and the data are reinverted. For 17 starting data we perform 16 separate inversions using 16 data (thin grey lines) compared to best fit results using all 17 data (heavy solid line).

microearthquake location are well illustrated in both map view (Figures 16 and 17) and cross section (Figure 3c); very few microearthquakes overlap the locked regions. Microearthquakes on or near the plate interface are restricted to the more freely slipping parts, while events within the upper plate tend to concentrate near the shallow transition from locked to more freely slipping regions. The distinct nature of the geodetically and microseismically defined updip limit of the seismogenic zone is a robust result: Our combined deployment of onshore and offshore seismometers means that the earthquakes are precisely located (horizontal uncertainties less than 1 km), while the geodetic results benefit from the dense station spacing and the fact that the Nicoya peninsula is located close to the trench, above most of the seismogenic zone, and as noted earlier are not sensitive to model details.

[46] All acceptable models also produce a down-dip locked or partly locked patch (Figures 11 and 13–15) although with less well constrained magnitude, extent and down-dip limit compared to the shallow patch. Microearthquakes in this region are somewhat diffuse, and may not all be plate interface events (our seismic array may also have reduced sensitivity here). Therefore we cannot rigorously assess the relation between geodetic and interseismic definitions of the down-dip seismogenic limit. To a first approximation, plate microseismicity and locking decrease significantly below 40 and 45 km respectively.

[47] The simplest interpretation of this pattern of locking versus microseismicity is that the shallow (10–15 km) locked patch is fully locked and does not produce significant microseismicity; below this, the plate interface transitions from fully locked to substantially slipping and is a locus for abundant interplate and nearby intraplate seismicity. If this pattern is generally true, it suggests that interseismic mircoearthquakes are a good way to outline the overall geometry of the plate boundary, but do not necessarily correspond to regions of high strain accumulation, and thus cannot reliably indicate the updip limit of the seismogenic zone, and may not reliably indicate the downdip limit of the seismogenic zone.

[48] Does the updip locked patch correspond to the updip limit of a future large earthquake? Figure 16 superimposes the aftershock areas of three past large earthquakes on the pattern of locked slip for the Nicoya region. The largest event was the 1950 Nicoya earthquake (M_s = 7.7); its epicentral location, along with the 1978 (M_w = 7.0) Sámara earthquake were recomputed by *Avants et al.* [2001] relative to the well-located 1990 (M_w =7.0) event [*Protti et al.*, 1995a]. *Protti et al.* [2001] suggested that the 1978 earthquake could have been a compressive intraplate event on the Cocos plate, based on its location, focal depth, and mechanism, reflecting bending of the oceanic plate due to a locked plate interface. However, relocation of the 1978 event refines its depth estimate, making it consistent with an interplate event. Although details of the coseismic slip distribution for the 1950 event are not known, the updip limit of the 1950 aftershock area appears to correspond with the updip edge of the currently locked patch.

[49] *Hyndman and Wang* [1993] and *Oleskovich et al.* [1999] suggested that the updip limit of the seismogenic zone corresponds to the 100–150°C isotherm. *Newman et al.* [2002] first suggested that the updip transition of the Nicoya boundary corresponds to this thermal boundary, as modeled by *Harris and Wang* [2002] and is likely affected by advective cooling of the oceanic crust in the northern portion of the peninsula. Using the more complete thermal model of *Spinelli and Saffer* [2004], we compared the updip locking limit and the microseismicity pattern in the Nicoya region to the location of the 100°C isotherm (Figure 17). This isotherm corresponds approximately to the updip limit of geodetically determined locking as well as the updip rupture limit of past large earthquakes (Figure 16). The thermal model of *Spinelli and Saffer* [2004] accounts for the abrupt difference in seafloor heat flow values obtained on East Pacific Rise (EPR) versus Cocos-Nazca Spreading Center (CNS) crust, including 1–2 km of hydrothermal cooling of EPR crust [*Fisher et al.*, 2003]. The offset in the 100°C isotherm, coincident with the change in oceanic crustal origin, is mimicked by a slight shallowing of the updip edge of the geodetically locked patch (Figure 17). If we define the updip limit of the seismogenic zone as the shallowest region able to accumulate significant strain (and hence likely to rupture seismically in a future earthquake), rather than the shallow limit of interseismic microearthquakes, these observations suggest that the updip limit at this location is controlled by thermally mediated diagenetic processes or low-grade metamorphic reactions near 100°C.

[50] An important question to be answered by future observations is the extent to which the distribution of locked slip and microearthquakes is time-transient. Perhaps the

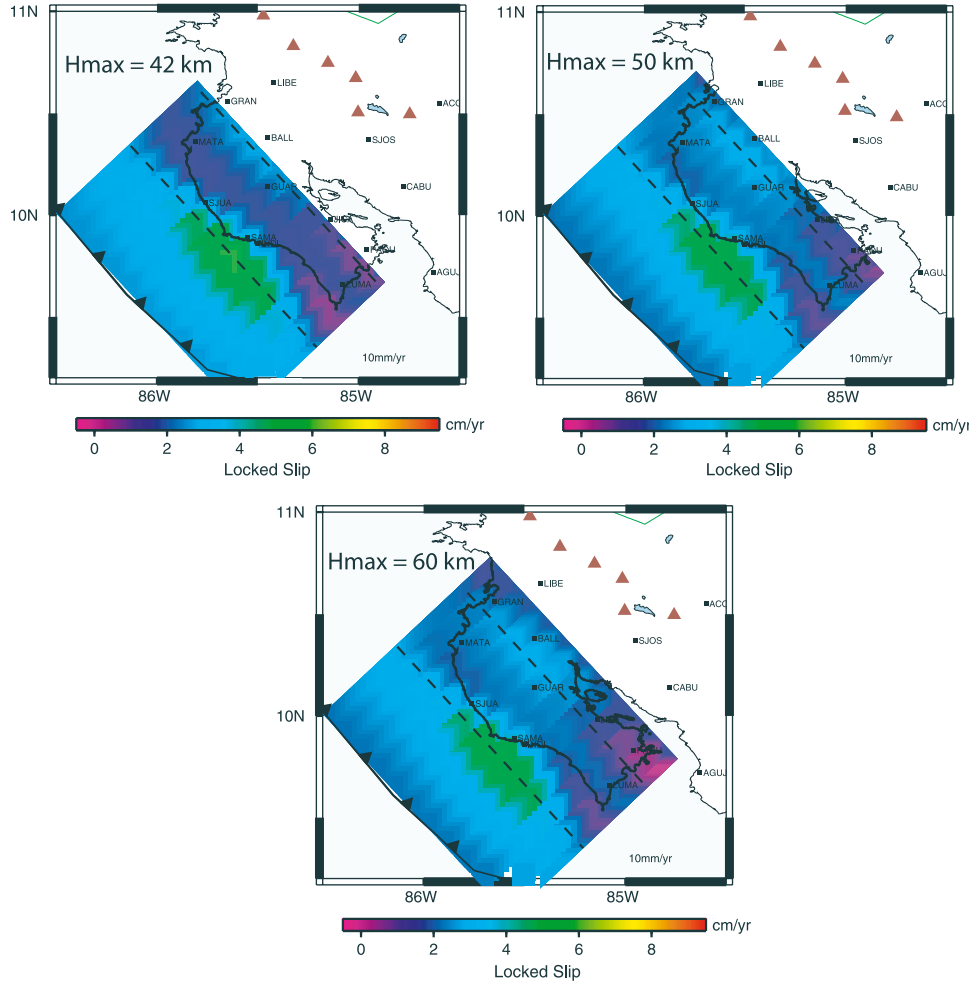

Figure 15. Variation in the location and magnitude of the deeper patch of locked slip as a function of the down-dip extent of the model plate interface for three down-dip limits: 42, 50, and 60 km.

patterns we observed would be different in different parts of the earthquake cycle.

7.2. Earthquake Cycle Deformation

[51] Spatial variability in coseismic slip during large earthquakes has been recognized for some time; however, the nature and persistence of regions of enhanced coseismic slip (asperities) and the behavior of the intervening weaker regions from one great earthquake to another and within an earthquake cycle are still unresolved. The simplest concept, known as the characteristic earthquake model, states that an earthquake is produced when a particular portion of the fault plane (asperity) fails in seismic rupture, with a recurrence interval equal to the time required for stress at that asperity to rebuild to a given level (presumably when its failure strength is exceeded). Assuming constant tectonic loading (stress rate), and either constant failure stress (constant material properties), final stress, or both, the slip and/or the recurrence time of future large earthquakes is thus predictable. These models have served as the basis for assessing long-term earthquake potential at active plate boundaries [e.g., *Jackson et al.*, 1995; *Nishenko*, 1991], although their validity has yet to be firmly established. Inherent in these models is persistent strong and weak parts of the fault zone through the interseismic part of the cycle and for consecutive large earthquakes. The implication is that weak regions slip relatively freely at or near the plate rate (generating abundant small earthquakes), loading the adjacent strong regions (that are completely locked) until failure occurs in a large earthquake. This concept has been used to identify asperities of future earthquakes from gaps in microseismicity patterns. For northeastern Japan, *Igarashi et al.* [2003] found that frequently repeating small earthquakes and adjacent freely slipping regions colocate with low-slip regions of coseismic moment release associated with two large plate boundary earthquakes in 1968 (M_w = 8.2) and 1994 (M_w = 7.7). Their distribution of "aseismic" slip (or "microseismic" slip) obtained from the repeating earthquakes also matches the pattern of freely slipping regions estimated from GPS. *Zweck et al.* [2002] document persistence of large asperities in the Alaska-Aleutian suduction zone, noting a correspondence between regions of interseismic strain accumulation and patches of high coseismic slip for the great 1964 (M_w = 9.2) Alaskan earthquake. These observations are consistent with a simple characteristic earthquake model, and persistence of locking patterns through more than one seismic cycle.

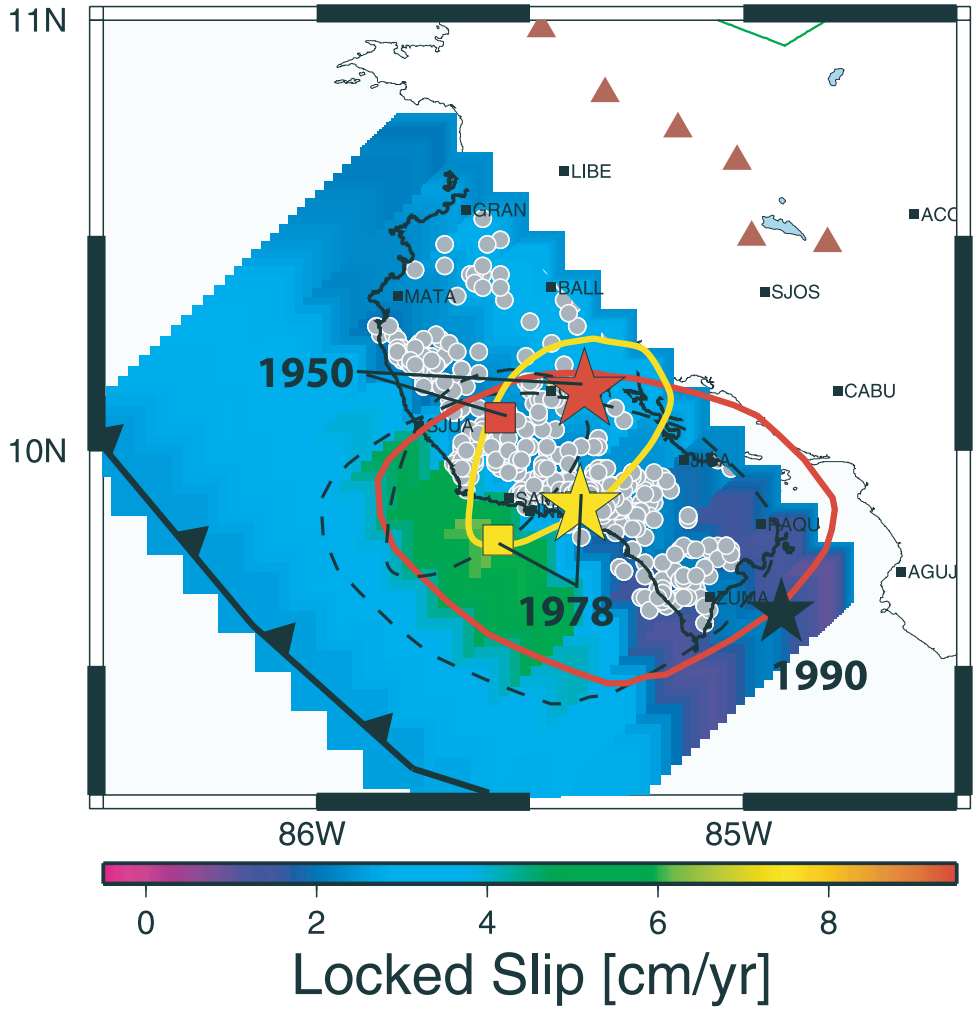

Figure 16. Comparison of distribution of locking from inversion of GPS data, well-located earthquakes from our seismic network, and rupture areas of past earthquakes. Original ISC (boxes) and relocated (stars) epicenters and corresponding rupture areas (dashed lines are original, colored solid lines are relocated) for the 1950 (M_w = 7.7; red) and 1978 (M_w = 7.0; yellow) Nicoya earthquakes. Epicenters and rupture areas are relocated relative to the well-located 1990 M_w = 7.0 Gulf of Nicoya event (black star) [*Avents et al.*, 2001].

[52] However, studies of other subduction zones have suggested that the location of strong and weak regions could vary between consecutive great earthquakes. *Schwartz* [1999] compared the spatial distribution of moment release for consecutive earthquake ruptures along four different subduction zones and found noncharacteristic behavior. While two of the earthquake pairs reruptured portions of the same asperity distribution, the other two events filled in areas of slip deficit left by preceding events. *Hirose and Hirahara* [2002] performed numerical simulations with realistic friction conditions and suggested that asperities with large dimensions along strike tend to only partially rupture in a given earthquake, so that long-term behavior may be complex. The Nicoya region may also exhibit complex behavior, even though the asperities here are relatively small. While the updip and down-dip limits are similar, the rupture area of the 1978 earthquake is less than half the area of the 1950 event, i.e., along strike rupture length can be highly variable.

[53] *Bilek et al.* [2003] related earthquake rupture complexity along the Costa Rican subduction zone to morphologic features on the subducting plate. For central Costa Rica, where incoming lithosphere is relatively rough, they suggested that seamounts or bathymetric highs subducted to seismogenic depths act as regions of enhanced locking. These regions should persist over many seismic cycles. However, in the Nicoya region, where incoming lithosphere is relatively smooth, the locked patches are elongated parallel to the trench, orthogonal to the orientation of seamount chains on the visible portion of the Cocos plate. Perhaps if subducting lithosphere is relatively smooth, temperature-controlled metamorphic phase changes and resulting changes in pore fluid pressure in the sediment column control locking.

[54] Additional evidence that locked portions of the plate interface may persist beyond a single earthquake cycle comes from extending the characteristic earthquake model to very small magnitude events. Small repeating earthquake

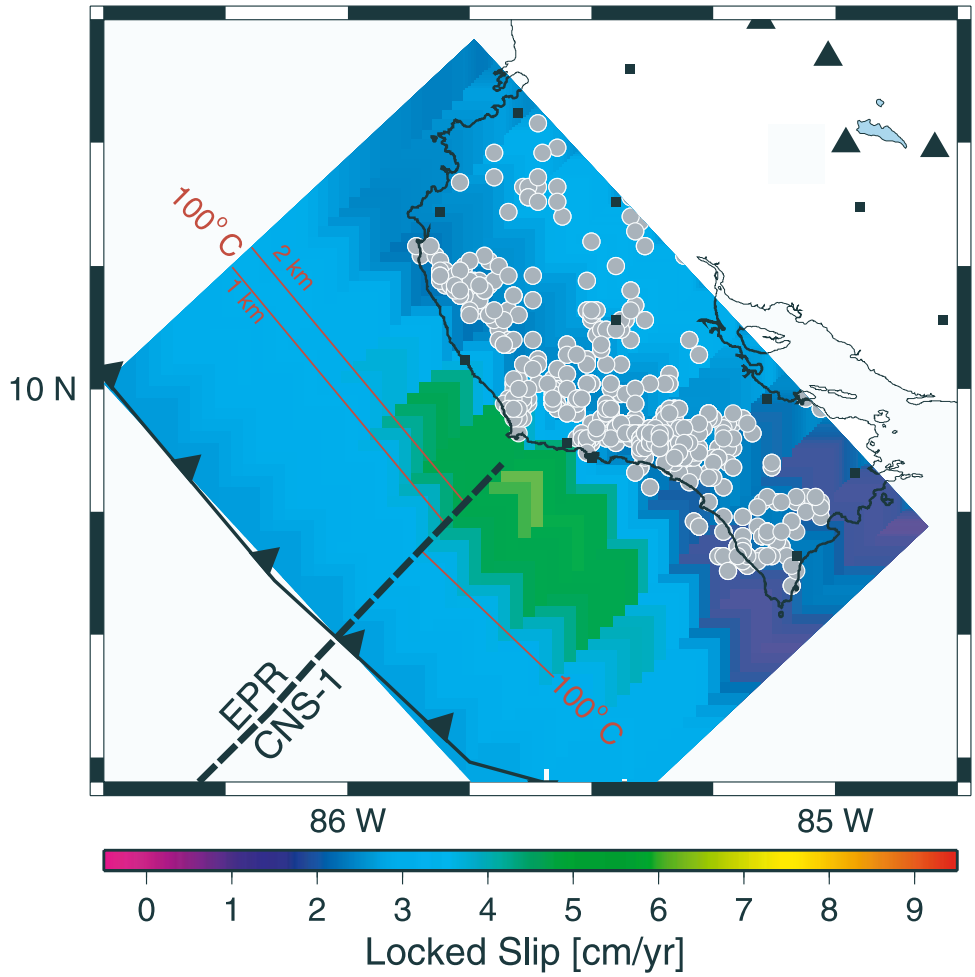

Figure 17. Comparison of well-located earthquakes from our seismic network, distribution of locking from inversion of GPS data, and 100°C isotherms from *Spinelli and Saffer* [2004]. For East Pacific Rise (EPR) crust, this is calculated assuming hydrothermal cooling of upper 1 and 2 km. Black triangles are active volcanoes. Earthquakes reach an updip limit about 50 km from the trench; maximum locking is centered about 35 km from the trench, approximately coincident with the 100°C isotherm that abruptly shallows across the boundary between crust generated at the EPR and Cocos-Nazca Spreading Center (CNS-1).

clusters in continental strike-slip zones [*Nadeau et al.*, 1995; *Nadeau and McEvilly*, 1998; *Bürgmann et al.*, 2000] have been interpreted as repeated failure of small asperities (with dimensions from 10 to 1000 m) driven by stable sliding of the intervening regions (the small events may be considered to have recurrence intervals of weeks to months). This has allowed determination of the spatiotemporal distribution of aseismic slip from the recurrence interval and estimated slip in the repeating earthquakes, and confirmed the essential aspects of a simple characteristic earthquake model for small events, at least over several seismic cycles.

7.3. Locked Versus Creeping Sections and Partial Coupling of the Seismogenic Zone

[55] The relation of microseismicity to locked and slipping patches observed in Nicoya has also been noted in continental strike-slip faults. *Nadeau and Johnson* [1988] compared the locations of repeating microearthquakes with locked and creeping patches on the Parkfield section of the San Andreas fault as defined by geodetic studies [*Harris and Segall*, 1987]. They found repeating microearthquakes concentrated in the creeping section. *Malservisi* [2002] reports concentrations of microearthquakes at transition zones between locked and more freely slipping regions of the Hayward fault in California, interpreted to indicate accelerated strain accumulation at the transitions. Increased strain at locked to creeping transition zones could deform the surrounding volume and explain abundant upper plate as well as interplate seismicity near the maximum gradient in locking (Figures 3c and 17).

[56] Many subduction zones have been determined to be "partially coupled" based on a comparison between seismic moment release rates and the full plate convergence rate [e.g., *Pacheco et al.*, 1993]. *McCaffrey* [1997] and *Norabuena et al.* [1998] discuss the difficulties inherent in these estimates. Partial coupling has also been reported in many geodetic studies [e.g., *Norabuena et al.*, 1998]. While we can generate a uniform slip solution in Nicoya with a partially locked seismogenic zone (approximately 35–

40% of the plate rate), the data density allows much finer resolution, and indicates that the seismogenic zone here is better represented by relatively small fully locked (or nearly so) patches, surrounded by regions that are essentially freely slipping. This suggests that some subduction thrusts, previously inferred to be partially coupled based on seismic data or spatially limited geodetic data, might be better represented by alternating locked and slipping regions; the degree of coupling would therefore represent the relative areas of these two contrasting types of mechanical behavior. Spatially dense geodetic data are required to investigate this issue.

[57] While our dense Nicoya network reduces spatial aliasing and suggests the presence of relatively small locked and slipping patches, our campaign observations will be temporally aliased if transient creep events occur [e.g., *Dragert et al.*, 2001]. For example, the relatively freely slipping patch beneath Nicoya where microseismicity is common might represent a locked zone that periodically experiences transient creep; sparse campaign observations would then record an intermediate level of strain accumulation, representing an average between locked and transient creep states. Continuous GPS stations are required to assess this possibility.

7.4. Longer Timescale Deformation

7.4.1. Trench-Parallel Forearc Block Motion

[58] We estimate trench-parallel motion of the Nicoya forearc to the northwest at a rate of 8 ± 3 mm/yr. *McCaffrey* [2002] inverted the data of *Lundgren et al.* [1999] for strain accumulation of the plate interface and rigid-body rotation of the forearc block assuming spherical geometry, obtaining 5 ± 6 mm/yr of forearc block motion (our estimate assumes simple Cartesian geometry, ignoring earth curvature which is small over the region of interest, but accounts for postseismic response to the 1992 Nicaragua earthquake). These two geodetic estimates are equivalent within uncertainties; both are slower than the 14 ± 2 mm/yr of block translation estimated by *DeMets* [2001] for the Nicaraguan forearc based on earthquake slip vector azimuths. Some of the difference may reflect the fact that both geodetic estimates in Costa Rica treat the Nicoya forearc as a single block, whereas it is possible that only the northern portion of the block translates at the higher rate inferred for Nicaragua. The geometry of the trench is such that oblique convergence is only defined for roughly the northern half of the Nicoya peninsula (Figure 1). For the southern half, convergence is essentially trench-normal. The geodetic estimates of Nicoya block translation rate (5–8 mm/yr) may therefore reflect an average between ~14 mm/yr to the north and essentially zero to the south. Higher spatial sampling of the surface velocity field, more sophisticated modeling and detailed geological mapping will be required to verify this and to define the region where northwest translation begins.

[59] The structures that might accommodate northwest block motion are not clear. Northwest striking right-lateral strike-slip faults are not well developed in northern Costa Rica, but could be obscured by recent volcanic deposits. Diffuse right-lateral shear could be accommodated within the thermally weak volcanic arc or the nearby Tempisque Basin (Figure 1). Block translation could also occur by vertical axis rotation of smaller blocks defined by short, northeast striking, left-lateral "bookshelf" faults, as proposed for Nicaragua [*LaFemina et al.*, 2002]. Our GPS data are not adequate to distinguish between these hypotheses. Focal mechanisms of smaller magnitude earthquakes recorded during our seismic deployment also do not show a clear pattern. However, several moderate magnitude historical earthquakes along the northern volcanic arc have damaged that region, in 1911 (between Arenal and Tenorio volcanoes), 1935 (Bagaces, southwest of Miravalles volcano), and 1973 (Tilaran, m_b = 5.7, right-lateral strike-slip on a northwest striking fault [*Guendel*, 1986]).

7.4.2. Crustal Shortening and Mountain Building

[60] The ~7 cm/yr of mean locked slip on the main plate boundary that we infer for the Osa segment is twice as high as the Nicoya segment (3.1 cm/yr, Table 4). Assuming these patterns are correct and extend over multiple seismic cycles, then this contrast in short-term mechanical behavior of the plate interface may explain differences in longer-term geologic processes (Table 4).

[61] The development of the western portion of the North Panama fold and thrust belt is generally ascribed to subduction of the aseismic Cocos Ridge [*Plafker and Ward*, 1992; *Suarez et al.*, 1995; *Collins et al.*, 1995; *Silver et al.*, 1995; *Tajima and Kikuchi*, 1995; *De Boer et al.*, 1995; *Kolarsky et al.*, 1995]. Development of the Fila Costeña may also relate to this event [*Protti et al.*, 1995b; *Fisher et al.*, 2004]. Both features are also probably influenced by the young (15–16 Ma) age of subducting lithosphere here. We suggest that the different locking patterns in the Osa and Nicoya regions similarly reflect the combined influence of contrasting seafloor age and subduction of the shallow Cocos Ridge [*Walther et al.*, 2000], in effect providing the mechanical link between long-term geological processes and the character of subducted seafloor. Subduction of the shallow Cocos ridge mimics the effect of young lithosphere, subduction of which is often associated with a high degree of locking [*Ruff and Kanamori*, 1980]. The combined effect of young age and shallow bathymetry implies that subducted lithosphere beneath Osa is anomalously buoyant, promoting mechanical coupling over a large depth range.

[62] Two other important differences between the regions are the presence of a volcanic arc and subduction obliquity in the north, and their absence in the south. Margin-parallel block transport in the north can be considered as a form of tectonic escape, perhaps insulating the back arc there from forearc compressive stresses, which are in any case small due to the relatively small area of locked patches on the plate interface. The presence of an active volcanic arc in the north may facilitate mechanical isolation of the back arc, representing a trench-parallel zone of weakness that helps to accommodate trench-parallel forearc motion. In the south, orthogonal convergence, lack of a volcanic arc, and lack of a tectonic escape mechanism means that the high compressive stresses associated with short-term elastic deformation and a fully locked plate boundary are transmitted through the rigid upper plate, promoting permanent crustal shortening in the upper plate wherever these stresses exceed some threshold for brittle failure.

7.4.3. Constraints on Timing

[63] Have differences in mechanical coupling between the two regions persisted long enough to influence geological

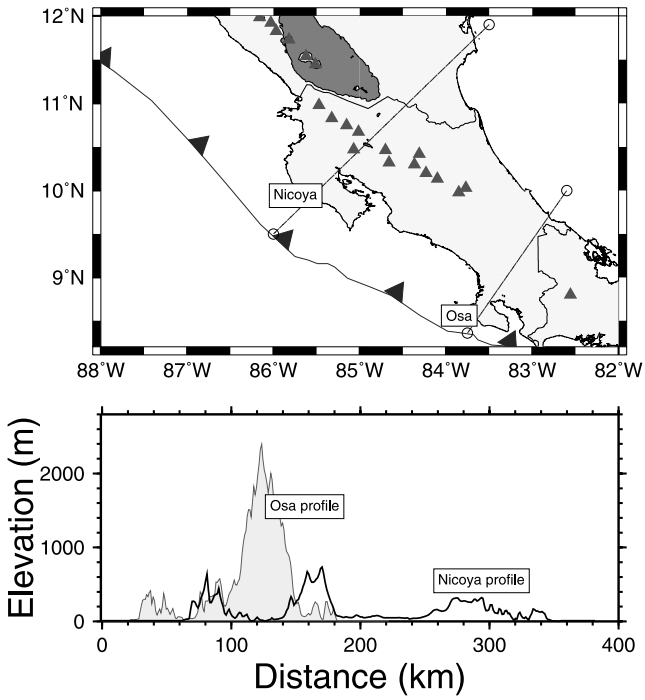

Figure 18. Topographic profiles for Osa and Nicoya.

development? If our hypothesis linking coupling with differences in seafloor age and subduction of the Cocos ridge is correct, this can be addressed in several ways. The relative age difference for subducted seafloor between Nicoya and Osa has persisted for at least the last few million years, based on analysis of magnetic lineations and plate reconstruction [*Barckhausen et al.*, 2001]. The Cocos Ridge began subducting sometime after 6 Myr, although there is uncertainty in the exact timing. *De Boer et al.* [1995] suggest initiation at about 5 Ma based on changes in arc magmatism. *Lonsdale and Klitgord* [1978] suggest initiation at about 1 Ma based on magnetic anomaly patterns on the Cocos plate. *Collins et al.* [1995] prefer an age of 3.6 Ma based on a detailed uplift history for the region from paleobathymetries of dated stratigraphic sections. Assuming 2 cm/yr of long-term shortening (sum of forearc and back-arc shortening) for the last 3 Myr gives 60 km of total shortening. *Fisher et al.* [2004] document a minimum of 17.4 km of shortening just in the Fila Costeña during the last 2–5 Myr. This process may have contributed to contrasts in mean elevation of the two regions (Figure 18) and perhaps crustal thickness.

8. Conclusions

[64] 1. The updip limit of the seismogenic zone in the Nicoya peninsula of Costa Rica, as determined from geodetic measurements of strain accumulation between 1994 and 2000, differs significantly from interseismic microseismicity recorded during 1999–2000. Geodetically determined locking begins at ~8 km depth and peaks at ~14 km depth. This is well updip of microseismicity but is close to the updip rupture limit of past large earthquakes.

[65] 2. The geodetically determined updip limit of the seismogenic zone corresponds approximately with *Spinelli and Saffer*'s [2004] 100°C isotherm. Both of these entities shallow across the change in oceanic crustal origin from the East Pacific Rise to the Cocos-Nazca Spreading Center.

[66] 3. Locked portions of the plate interface in the Nicoya area do not experience significant microseismicity during the interseismic part of the earthquake cycle; more freely slipping regions do experience microseismicity. If this pattern persists through the entire interseismic part of the cycle, then the locked portions can be expected to contribute significant moment (i.e., rupture with large slip) in the next major earthquake, while the microseismic regions would presumably rupture by smaller amounts and contribute less moment.

[67] 4. The Nicoya forearc block translates northwest at an average rate of 8 ± 3 mm/yr.

[68] 5. Relative plate motion in the Osa region of Costa Rica is partitioned between the Pacific (Cocos-Panama block) boundary, accommodating ~8 cm/yr (~1 cm/yr of permanent shortening across the Fila Costeña fold and thrust belt, ~7 cm/yr of elastic strain accumulation on the main plate boundary), and the Caribbean (Panama block-Caribbean plate) boundary, accommodating ~1 cm/yr.

[69] **Acknowledgments.** We thank NSF's MARGINS program (grants OCE 99 05469 to T.H.D., OCE9910609 to S.Y.S., and OCE9910350 to L.M.D.) and Germany's BMBF (grant 03G0144) and SFB 574 of Christian Albrechts University of Kiel for providing funds for these joint marine and on-land observations. We thank personnel of the F/S *Sonne* and R/V *Melville* for deployment and recovery of the OBS and OBH. Some of the land seismic instrumentation was provided by the PASSCAL facility of the Incorporated Research Institutions for Seismology (IRIS) through the PASSCAL instrument center at New Mexico Tech. Data from these stations are available through the IRIS Data Management Center. Many of the GPS receivers, and technical assistance for their deployment, were provided by UNAVCO. The GPS data are available at the UNAVCO archive. We also thank personnel at OVSICORI-UNA, including E. Hernandez, R. van der Laat, and Tomas Marino for their assistance in GPS and seismic data collection. Reviews by Seth Stein, Stephane Mazzotti, and Jeff Freymueller significantly improved the manuscript.

References

Adamek, S., F. Tajima, and D. Wiens (1987), Seismic rupture associated with subduction of the Cocos Ridge, *Tectonics*, *6*, 757–774.

Avants, M., S. Schwartz, A. Newman, and H. DeShon (2001), Large underthrusting earthquakes beneath the Nicoya Peninsula, *Eos Trans. AGU*, *82*(46), Fall Meet. Suppl., Abstract T52E-07.

Barckhausen, U., C. R. Ranero, R. von Huene, S. C. Cande, and H. A. Roeser (2001), Revised tectonic boundaries in the Cocos plate off Costa Rica: Implications for the segmentation of the convergent margin and for plate tectonic models, *J. Geophys. Res.*, *106*, 19,207–19,220.

Beck, M. E., Jr. (1991), Coastwise transport reconsidered: Lateral displacements in oblique subduction zones, and tectonic consequences, *Phys. Earth Planet. Inter.*, *68*, 1–8.

Beck, M. E., Jr., R. E. Burmester, R. E. Drake, and P. D. Riley (1994), A tale of two continents: Some tectonic contrasts between the central Andes and the North American Cordillera, as illustrated by their paleomagnetic signatures, *Tectonics*, *13*, 215–224.

Bialas, J., E. R. Flueh, and G. Bohrmann (Eds.) (1999), FS *Sonne* cruise report SO144/1&2: PAGANINI, *GEOMAR Rep. 102*, 437 pp., GEOMAR, Kiel, Germany.

Bilek, S. L., S. Y. Schwartz, and H. R. DeShon (2003), Control of seafloor roughness on earthquake rupture behavior, *Geology*, *31*, 455–458.

Boucher, C., Z. Altamimi, and P. Sillard (1999), The 1997 International Terrestrial Reference Frame (ITRF-97), *IERS Tech. Note, 27*, Obs. de Paris, Paris.

Bürgmann, R., D. Schmidt, R. M. Nadeau, M. d'Alessio, E. Fielding, D. Manaker, T. V. McEvilly, and M. H. Murray (2000), Earthquake potential along the northern Hayward fault, California, *Science*, *289*, 1178–1181.

Case, J. E., and T. L. Holcombe (1980), Geologic map of the Caribbean region, *U.S. Geol. Surv. Misc. Invest. Map, I-1100*, scale 1:2,500,000.

Christeson, G. L., K. D. McIntosh, T. H. Shipley, E. R. Flueh, and H. Goedde (1999), Structure of the Costa Rica convergent margin, offshore Nicoya Peninsula, *J. Geophys. Res.*, *104*(11), 25,443–25,468.

Collins, L. S., A. Coates, J. Jackson, and J. Obando (1995), Timing and rates of emergence of the Limon and Bocas del Toro basins: Caribbean effects of Cocos Ridge subduction?, in *Geologic and Tectonic Development of the Caribbean Plate Boundary in South America*, edited by P. Mann, *Spec. Pap. Geol. Soc. Am.*, *295*, 263–290.

De Boer, J. Z., M. S. Drummond, M. J. Bordelon, M. J. Defant, H. Bellon, and R. C. Maury (1995), Cenozoic magmatic phases of the Costa Rican island arc (Cordillera de Talamanca)?, in *Geologic and Tectonic Development of the Caribbean Plate Boundary in South America*, edited by P. Mann, *Spec. Pap. Geol. Soc. Am.*, *295*, 35–55.

DeMets, C. (2001), A new estimate for Cocos-Caribbean plate motion: Implications for slip along the Central American volcanic arc, *Geophys. Res. Lett.*, *28*, 4043–4046.

DeMets, C., R. G. Gordon, D. F. Argus, and S. Stein (1990), Current plate motions, Geophys, *J. Int.*, *101*, 425–478.

DeMets, C., R. G. Gordon, D. F. Argus, and S. Stein (1994), Effect of recent revisions to the geomagnetic time scale on estimates of current plate motion, *Geophys. Res. Lett.*, *21*, 2191–2194.

DeShon, H. R. (2004), Seismogenic zone structure along the Middle America subduction zone, Costa Rica, Ph.D. thesis, 330 pp., Univ. of Calif., Santa Cruz.

DeShon, H. R., S. Y. Schwartz, S. L. Bilek, L. M. Dorman, V. Gonzalez, J. M. Protti, E. R. Flueh, and T. H. Dixon (2003), Seismogenic zone structure of the southern Middle America Trench, Costa Rica, *J. Geophys. Res.*, *108*(B10), 2491, doi:10.1029/2002JB002294.

Dixon, T. H. (1993), GPS measurements of relative motion of the Cocos and Caribbean plates and strain accumulation across the Middle America Trench, *Geophys. Res. Lett.*, *20*, 2167–2170.

Dixon, T. H., and S. K. Wolf (1990), Some tests of wet tropospheric calibration for the Casa Uno GPS experiment, *Geophys. Res. Lett.*, *17*, 203–206.

Dixon, T. H., M. Miller, F. Farina, H. Wang, and D. Johnson (2000), Present-day motion of the Sierra Nevada block and some tectonic implications for the Basin and Range province, North American Cordillera, *Tectonics*, *19*, 1–24.

Dixon, T., J. Decaix, F. Farina, K. Furlong, R. Malservisi, R. Bennett, F. Suarez-Vidal, J. Fletcher, and J. Lee (2002), Seismic cycle and rheological effects on estimation of present-day slip rates for the Agua Blanca and San Miguel-Vallecitos faults, northern Baja California, Mexico, *J. Geophys. Res.*, *107*(B10), 2226, doi:10.1029/2000JB000099.

Dragert, H., K. Wang, and T. S. James (2001), A silent slip event on the deeper Cascadia subduction interface, *Science*, *292*, 1525–1528.

Fisher, A. T., C. A. Stein, R. N. Harris, K. Wang, E. A. Silver, M. Pfender, M. Hutnak, A. Cherkaoui, R. Bodzin, and H. Villinger (2003), Abrupt thermal transition reveals hydrothermal boundary and role of seamounts within the Cocos plate, *Geophys. Res. Lett.*, *30*(11), 1550, doi:10.1029/2002GL016766.

Fisher, D. M., T. W. Gardner, P. B. Sak, J. D. Sanchez, K. Murphy, and P. Vannucchi (2004), Active thrusting in the inner forearc of an erosive convergent margin, Pacific coast, Costa Rica, *Tectonics*, *23*, TC2007, doi:10.1029/2002TC001464.

Fitch, T. J. (1972), Plate convergence, transcurrent faults, and internal deformation adjacent to Southeast Asia and western Pacific, *J. Geophys. Res.*, *77*, 4432–4460.

Goes, S. D. B., A. A. Velasco, S. Y. Schwartz, and T. Lay (1993), The April 22, 1991 Valle de la Estrella, Costa Rica (M_w = 7.7) earthquake and its tectonic implications: A broadband seismic study, *J. Geophys. Res.*, *98*, 8127–8142.

Guendel, F. (1986), Seismotectonics of Costa Rica: An analytical view of the southern terminus of the Middle America Trench, Ph.D. thesis, Univ. of Calif., Santa Cruz.

Harris, R. N., and P. Segall (1987), Detection of a locked zone at depth on the Parkfield, California segment of the San Andreas fault, *J. Geophys. Res.*, *92*, 7945–7962.

Harris, R. N., and K. Wang (2002), Thermal models of the Middle America Trench at the Nicoya Peninsula, Costa Rica, *Geophys. Res. Lett.*, *29*(21), 2010, doi:10.1029/2002GL015406.

Hirth, G., and D. L. Kohlstedt (1996), Water in the oceanic upper mantle: Implications for rheology, melt extraction and the evolution of the lithosphere, *Earth Planet. Sci. Lett.*, *144*, 93–108.

Hirose, H., and K. Hirahara (2002), A model for complex slip behavior on a large asperity at subduction zones, *Geophys. Res. Lett.*, *29*(22), 2068, doi:10.1029/2002GL015825.

Hyndman, R. D., and K. Wang (1993), Thermal constraints on the zone of major thrust earthquake failure: The Cascadia subduction zone, *J. Geophys. Res.*, *98*, 2039–2060.

Hyndman, R. D., and K. Wang (1995), The rupture zone of Cascadia great earthquakes from current deformation and the thermal regime, *J. Geophys. Res.*, *100*, 22,133–22,154.

Hyndman, R. D., K. Wang, and M. Yamano (1995), Thermal constraints on the seismogenic portion of the southwest Japan subduction thrust, *J. Geophys. Res.*, *100*, 15,373–15,392.

Ide, S., F. Imamura, Y. Yoshida, and K. Abe (1993), Source characteristics of the Nicaragua tsunami earthquake of September 2, 1992, *Geophys. Res. Lett.*, *20*, 863–866.

Igarashi, T., T. Matsuzawa, and A. Hasegawa (2003), Repeating earthquakes and interplate aseismic slip in the northeastern Japan subduction zone, *J. Geophys. Res.*, *108*, 2249, doi:10.1029/2002JB001920.

Ihmle, P. F. (1996), Frequency-dependent relocation of the 1992 Nicaragua slow earthquake: An empirical Green's function approach, *Geophys. J. Int.*, *127*, 75–85.

Imamura, F., N. Shuto, S. Ide, Y. Yoshida, and K. Abe (1993), Estimate of the tsunami source of the 1992 Nicaragua earthquake from tsunami data, *Geophys. Res. Lett.*, *20*, 1515–1518.

Jackson, D. D., K. Aki, C. A. Cornell, J. H. Dietrich, T. L. Henyey, M. Mahdyiar, D. Schwart, and S. N. Ward (1995), Seismic hazards in southern California; probable earthquakes, 1994–2024, *Bull. Seismol. Soc. Am.*, *85*, 379–439.

Jacobson, R. S., L. M. Dorman, M. Purdy, A. Schultz, and S. C. Solomon (1991), Ocean bottom seismometer facilities available, *Eos Trans. AGU*, *72*(46), 505, 515.

James, T. S., J. J. Clague, K. Wang, and I. Hutchinson (2000), Post-glacial rebound at the northern Cascadia subduction zone, *Quat. Sci. Rev.*, *19*, 1527–1541.

Jarrard, R. D. (1986), Relations among subduction parameters, *Rev. Geophys.*, *24*, 217–284.

Kanamori, H. (1972), Mechanism of tsunami earthquakes, *Phys. Earth Planet. Inter.*, *6*, 246–259.

Kanamori, H., and M. Kikuchi (1993), The 1992 Nicaragua earthquake: A slow tsunami earthquake associated with subducted sediment, *Nature*, *361*, 714–715.

Kikuchi, M., and H. Kanamori (1995), Source characteristics of the 1992 Nicaragua tsunami earthquake inferred from teleseismic body waves, *Pure Appl. Geophys.*, *144*, 441–453.

Kohlstedt, D. L., B. Evans, and S. J. Mackwell (1995), Strength of the lithosphere: Constraints imposed by laboratory experiments, *J. Geophys. Res.*, *100*, 17,587–17,602.

Kolarsky, R. A., P. Mann, W. Montero (1995), Island arc response to shallow subduction of the Cocos Ridge, Costa Rica, in *Geologic and Tectonic Development of the Caribbean Plate Boundary in South America*, edited by P. Mann, *Spec. Pap. Geol. Soc. Am.*, *295*, 235–262.

LaFemina, P. C., T. H. Dixon, and W. Strauch (2002), Bookshelf faulting in Nicaragua, *Geology*, *30*, 751–754.

Langseth, M. G., and E. A. Silver (1996), The Nicoya convergent margin-a region of exceptionally low heat flow, *Geophys. Res. Lett.*, *23*, 891–894.

Lonsdale, P., and K. D. Klitgord (1978), Structure an tectonic history of the eastern Panama Basin, *Geol. Soc. Am. Bull.*, *89*, 981–999.

Lundgren, P., S. Wolf, M. Protti, and K. Hurst (1993), GPS measurements of crustal deformation following the 22 April 1991 Valle de Estrella Costa Rica earthquake, *Geophys. Res. Lett.*, *20*, 407–410.

Lundgren, P., M. Protti, A. Donnellan, M. Heflin, E. Hernandez, and D. Jefferson (1999), Seismic cycle and plate margin deformation in Costa Rica: GPS observations from 1994 to 1997, *J. Geophys. Res.*, *104*, 28,915–28,928.

Malservisi, R. (2002), Numerical models of the dynamics of lithospheric deformation at complex plate boundaries, Ph.D. thesis, 120 pp., Penn. State Univ., State College.

Mao, A., G. G. H. Harrison, and T. Dixon (1999), Noise in GPS coordinate time series, *J. Geophys. Res.*, *104*, 2797–2816.

Marshall, J. S., D. M. Fisher, and T. W. Gardner (2000), Central Costa Rica deformed belt: Kinematics of diffuse faulting across the western Panama block, *Tectonics*, *19*, 468–492.

McCaffrey, R. (1992), Oblique plate convergence, slip vectors, and forearc deformation, *J. Geophys. Res.*, *97*, 8905–8915.

McCaffrey, R. (1997), Statistical significance of the seismic coupling coefficient, *Bull. Seismol. Soc. Am.*, *87*, 1069–1073.

McCaffrey, R. (2002), Crustal block rotations and plate coupling, in *Plate Boundary Zones*, *Geodyn. Ser.*, vol. 20, edited by S. Stein and J. Freymueller, pp. 101–122, AGU, Washington, D. C.

Murdoch, J. N. (2003), Comment on Discussions of ODP Leg 205 and drilling of Middle America seismogenic zone, *Eos Trans. AGU*, *84*, 303.

Nadeau, R. M., and L. R. Johnson (1988), Seismological studies at Parkfield, VI: Moment release rates and estimates of source parameters for small repeating earthquakes, *Bull. Seismol. Soc. Am.*, *88*, 790–814.

Nadeau, R. M., and T. V. McEvilly (1998), Fault slip rates at depth from recurrence intervals of repeating microearthquakes, *Science*, *285*, 718–721.

Nadeau, R. M., W. Foxhall, and T. V. McEvilly (1995), Clustering and periodic recurrence of microearthquakes on the San Andreas fault at Parkfield, California, *Science*, *267*, 503–507.

Newman, A. V., S. Y. Schwartz, V. Gonzalez, H. R. DeShon, J. M. Protti, and L. M. Dorman (2002), Along-strike variability in the seismogenic zone below Nicoya Peninsula, Costa Rica, *Geophys. Res. Lett.*, *29*(20), 1977, doi:10.1029/2002GL015409.

Nicol, A., and J. Beavan (2003), Shortening of an overriding plate and its implications for slip on a subduction thrust, central Hikurangi Margin, New Zealand, *Tectonics*, *22*(6), 1070, doi:10.1029/2003TC001521.

Nishenko, S. P. (1991), Circum-Pacific seismic potential, 1989–1999, *Pure Appl. Geophys.*, *135*, 169–259.

Norabuena, E. (2004), Space geodetic studies of crustal deformation in subduction zones: The central Andes and Costa Rica, Ph.D. thesis, 110 pp., Univ. of Miami, Coral Gables.

Norabuena, E., L. Leffler, A. Mao, T. Dixon, S. Stein, S. Sacks, and M. Ellis (1998), Space geodetic observation of Nazca-South America convergence along the central Andes, *Science*, *279*, 358–362.

Norabuena, E. O., T. H. Dixon, S. Stein, and C. G. A. Harrison (1999), Decelerating Nazca-South America and Nazca-Pacific plate motions, *Geophys. Res. Lett.*, *26*, 3405–3408.

Obana, K., S. Kodaira, Y. Kaneda, K. Mochizuki, M. Shinohara, and K. Suyehiro (2003), Microseismicity at the seaward updip limit of the western Nankai Trough seismogenic zone, *J. Geophys. Res.*, *108*(B10), 2459, doi:10.1029/2002JB002370.

Oleskevich, D. A., R. D. Hyndman, and K. Wang (1999), The updip and downdip limits to great subduction earthquakes: Thermal and structural models of Cascadia, south Alaska, SW Japan and Chile, *J. Geophys. Res.*, *104*, 14,965–14,991.

Pacheco, J. F., L. Sykes, and C. Scholz (1993), Nature of seismic coupling along simple plate boundaries of the subduction type, *J. Geophys. Res.*, *98*, 14,133–14,159.

Peacock, S. (1993), Large-scale hydration of the lithosphere above subducting slabs, *Chem. Geol.*, *108*, 49–59.

Peltier, W. R. (1998), Postglacial variations in the level of the sea: Implications for climate dynamics and solid earth geophysics, *Rev. Geophys.*, *36*, 603–689.

Plafker, G., and S. N. Ward (1992), Thrust faulting and tectonic uplift along the April 22, 1991 Costa Rico earthquake, *Tectonics*, *11*, 709–718.

Pollitz, F. F. (1997), Gravitational viscoelastic postseismic relaxation on a layered spherical Earth, *J. Geophys. Res.*, *102*, 17,921–17,941.

Pollitz, F. F., R. Burgmann, and P. Segall (1998), Joint estimation of afterslip rate and postseismic relaxation following the 1989 Loma Prieta earthquake, *J. Geophys. Res.*, *103*, 26,975–26,992.

Protti, M., and S. Schwartz (1994), Mechanics of back arc deformation in Costa Rica, *Tectonics*, *13*, 1093–1107.

Protti, M., F. Guendel, and K. McNally (1994), Geometry of the Wadati-Benioff zone under South America and its tectonic significance, *Phys. Earth Planet. Inter.*, *84*, 271–287.

Protti, M., et al. (1995a), The March 25, 1990 (M_w = 7.0, M_L = 6.8), earthquake at the entrance of the Nicoya Gulf, Costa Rica: Its prior activity, foreshocks, aftershocks, and triggered seismicity, *J. Geophys. Res.*, *100*(10), 20,345–20,358.

Protti, M., F. Guendel, and K. McNally (1995b), Correlation between the age of the subducting Cocos plate and the geometry of the Wadati-Benioff zone under Nicaragua and Costa Rica, in *Geologic and Tectonic Development of the Caribbean Plate Boundary in Southern Central America*, edited by P. Mann, *Spec. Pap. Geol. Soc. Am.*, *295*, 309–326.

Protti, M., F. Güendel, and E. Malavassi (2001), Evaluación del Potencial Sıacute;smico de la Penıacute;nsula de Nicoya, 1st ed., 144 pp., Ed. Fundación Univ. Nac. Auton., Heredia, Costa Rica.

Ranero, C. R., and R. von Huene (2000), Subduction erosion along the Middle America convergent margin, *Nature*, *404*, 748–752.

Ruff, L., and H. Kanamori (1980), Seismicity and the subduction process, *Phys. Earth Planet. Inter.*, *23*, 240–252.

Ruff, L., and B. W. Tichelaar (1996), What controls the seismogenic plate interface in subduction zones, in *Subduction Top to Bottom*, *Geophys. Monogr. Ser.*, vol. 96, edited by G. E. Bebout et al., pp. 105–111, AGU, Washington, D. C.

Sallarès, V., J. J. Dañobeitia, E. R. Flueh, and G. Leandro (1999), Seismic velocity structure across the Middle American landbridge in northern Costa Rica, *J. Geodyn.*, *27*, 327–344.

Sallarès, V., J. J. Dañobeitia, and E. R. Flueh (2000), Seismic tomography with local earthquakes in Costa Rica, *Tectonophysics*, *329*, 61–78.

Sallarès, V., J. J. Dañobeitia, and E. R. Flueh (2001), Lithospheric structure of the Costa Rica Isthmus: Effects of subduction zone magmatism on an oceanic plateau, *J. Geophys. Res.*, *106*, 621–643.

Satake, K. (1994), Mechanism of the 1992 Nicaragua tsunami earthquake, *Geophys. Res. Lett.*, *21*, 2519–2522.

Satake, K. (1995), and nonlinear computations of the 1992 Nicaragua earthquake tsunami, *Pure Appl. Geophys.*, *144*, 455–470.

Sauter, A. W., J. Hallinan, R. Currier, T. Barash, B. Wooding, A. Schultz, and L. M. Dorman (1990), A new ocean bottom seismometer, in *Marine Instrumentation '90 Conference Proceedings*, pp. 99–104, Mar. Technol. Soc., Columbia, Md.

Savage, J. C. (1983), A dislocation model of strain accumulation and release at a subduction zone, *J. Geophys. Res.*, *88*, 4984–4996.

Schwartz, S. Y. (1995), Source parameters of aftershocks of the 1991 Costa Rica and 1992 Cape Mendocino, California earthquakes from inversion of local amplitude ratios and broadband waveforms, *Bull. Seismol. Soc. Am.*, *85*, 1560–1575.

Schwartz, S. Y. (1999), Non-characteristic behavior and complex recurrence of large subduction zone earthquakes, *J. Geophys. Res.*, *104*, 23,111–23,125.

Schwartz, S. Y., A. V. Newman, M. Protti, and M. Vallee (2001), A large tensional outer-rise earthquake in the Nicoya seismic gap, Costa Rica, *Eos Trans. AGU*, *82*(47), Fall Meet. Suppl., Abstract S12B-0600.

Sella, G. F., T. H. Dixon, and A. Mao (2002), REVEL: A model for Recent plate velocities from space geodesy, *J. Geophys. Res.*, *107*(B4), 2081, doi:10.1029/2000JB000033.

Silver, E. A., D. L. Reed, J. E. Tagudin, and D. J. Heil (1990), Implications of the north and south Panama thrust belts for the origin of the Panama orocline, *Tectonics*, *9*, 261–281.

Silver, E. A., J. Galewsky, and K. D. McIntosh (1995), Variation in structure, style and driving mechanism of adjoining segments of the North Panama deformed belt, in *Geologic and Tectonic Development of the Caribbean Plate Boundary in South America*, edited by P. Mann, *Spec. Pap. Geol. Soc. Am.*, *295*, 225–234.

Spinelli, G. A., and D. M. Saffer (2004), Along-strike variations in underthrust sediment dewatering on the Nicoya margin, Costa Rica related to the updip limit of seismicity, *Geophys. Res. Lett.*, *31*, L04613, doi:10.1029/2003GL018863.

Stavenhagen, A. U., E. R. Flueh, C. Ranero, K. D. McIntish, T. Shipley, G. Leandro, A. Schulze, and J. J. Danobeitia (1998), Seismic wide angle investigations in Costa Rica: A crustal velocity model from the Pacific to Caribbean coast, *Z. Geol. Palaontol.*, *1*(3–6), 393–406.

Suarez, G., M. Pardo, J. Dominguez, L. Ponce, W. Montero, I. Boschini, and W. Rojas (1995), The Limon, Costa Rica earthquake of April 22, 1991: Back arc thrusting and collisional tectonics in a subduction environment, *Tectonics*, *14*, 518–530.

Tajima, F., and M. Kikuchi (1995), Tectonic implications of the seismic ruptures associated with the 1983 and 1991 Costa Rica earthquakes, in *Geologic and Tectonic Development of the Caribbean Plate Boundary in South America*, edited by P. Mann, *Spec. Pap. Geol. Soc. Am.*, *295*, 327–340.

Vergara-Munoz, A. (1988), Tectonic patterns of the Panama Block deduced from seismicity, gravitational data and earthquake mechanisms: Implications to the seismic hazard, *Tectonophysics*, *154*, 253–267.

Von Huene, R., et al. (1995), Morphotectonics of the Pacific convergent margin of Costa Rica, in *Geologic and Tectonic Development of the Caribbean Plate Boundary in South America*, edited by P. Mann, *Spec. Pap. Geol. Soc. Am.*, *295*, 291–307.

Walther, C. H. E. (2003), The crustal structure of Cocos Ridge off Costa Rica, *J. Geophys. Res.*, *108*(B3), 2136, doi:10.1029/2001JB000888.

Walther, C., and E. Flueh (2002), Remnant of the ancient Farallon plate breakup: A low-velocity body in the lower oceanic crust off Nicoya Peninsula, Costa Rica-Evidence from wide-angle seismics, *Geophys. Res. Lett.*, *29*(19), 1939, doi:10.1029/2002GL015026.

Walther, C. H. E., E. R. Flueh, C. R. Ranero, R. von Huene, and W. Strauch (2000), Crustal structure across the Pacific margin of Nicaragua: Evidence for ophiolitic basement and a shallow mantle sliver, *Geophys. J. Int.*, *141*, 759–777.

Wang, K., and T. H. Dixon (2004), Coupling semantics and science in earthquake research, *Eos Trans. AGU*, *85*, 180.

Ye, S., J. Bialas, E. R. Flueh, A. Stavenhagen, R. von Huene, G. Leandro, and K. Hinz (1996), Crustal structure of the Middle American Trench off Costa Rica from wide-angle seismic data, *Tectonics*, *15*, 1006–1021.

Zweck, C., J. T. Freymueller, and S. C. Cohen (2002), Three-dimensional elastic dislocation modeling of the postseismic response to the 1964 Alaska earthquake, *J. Geophys. Res.*, *107*(B4), 2064, doi:10.1029/2001JB000409.

H. DeShon, Department of Geology and Geophysics, University of Wisconsin-Madison, 1215 W Dayton St., Madison, WI 53706, USA.

T. H. Dixon (corresponding author) and E. Norabuena, Rosenstiel School of Marine and Atmospheric Sciences, University of Miami, 4600

Rickenbacker Causeway, Miami, FL 33149, USA. (tdixon@rsmas.miami.edu; enorabueana@rsmas.miami.edu)

L. Dorman, Scripps Institution of Oceanography, University of California, San Diego, La Jolla, CA 92093, USA. (dorman@jewel.ucsd.edu)

E. R. Flueh, Leibniz Institut fur Meereswissenshaften, IFM-GEOMAR, WischofstasseStr 1-3, D-24148 Kiel, Germany. (eflueh@ifm-geomar.de)

V. Gonzalez and M. Protti, Observatorio Vulcanológico y Sismológico de Costa Rica, Universidad Nacional, Apartado 2346-3000, Heredia, Costa Rica. (jprotti@una.ac.cr)

P. Lundgren, Jet Propulsion Laboratory, California Institute of Technology, 4800 Oak Grove Drive, Pasadena, CA 91109-8099, USA. (paul@weed.jpl.nasa.gov)

A. Newman, Los Alamos National Laboratory, Earth and Environmental Sciences Division, MS-D462, Los Alamos, NM 87545, USA. (anewman@lanl.gov)

F. Pollitz, U.S. Geological Survey, 345 Middlefield Road, MS 977, Menlo Park, CA 94025, USA. (fpollitz@usgs.gov)

D. Sampson and S. Schwartz, Earth Sciences Department, University of California, Santa Cruz, CA 95064, USA. (sschwartz@es.ucsc.edu)